AD_____

AWARD NUMBER: DAMD17-03-1-0224

TITLE: Angiogenesis and therapeutic approaches to NF1 tumors

PRINCIPAL INVESTIGATOR: David F. Muir, Ph.D.

CONTRACTING ORGANIZATION: University of Florida
Gainesville, Florida 32611

REPORT DATE: April 2006

TYPE OF REPORT: Annual

PREPARED FOR: U.S. Army Medical Research and Materiel Command
Fort Detrick, Maryland 21702-5012

REPORT DOCUMENTATION PAGE

Form Approved
OMB No. 0704-0188

1. REPORT DATE *(DD-MM-YYYY)*	**2. REPORT TYPE**	**3. DATES COVERED** *(From - To)*
April 2006	Annual	1 Apr 05 – 31 Mar 06

4. TITLE AND SUBTITLE

Angiogenesis and therapeutic approaches to NF1 tumors

5a. CONTRACT NUMBER

5b. GRANT NUMBER
DAMD17-03-1-0224

5c. PROGRAM ELEMENT NUMBER

6. AUTHOR(S)

David F. Muir, Ph.D.

E-Mail: muir@ufbi.ufl.edu

5d. PROJECT NUMBER

5e. TASK NUMBER

5f. WORK UNIT NUMBER

7. PERFORMING ORGANIZATION NAME(S) AND ADDRESS(ES)

University of Florida
Gainesville, Florida 32611

8. PERFORMING ORGANIZATION REPORT NUMBER

9. SPONSORING / MONITORING AGENCY NAME(S) AND ADDRESS(ES)
U.S. Army Medical Research and Materiel Command
Fort Detrick, Maryland 21702-5012

10. SPONSOR/MONITOR'S ACRONYM(S)

11. SPONSOR/MONITOR'S REPORT NUMBER(S)

12. DISTRIBUTION / AVAILABILITY STATEMENT
Approved for Public Release; Distribution Unlimited

13. SUPPLEMENTARY NOTES

14. ABSTRACT

The main goal of this project is to specify how anti-angiogenic approaches can be effectively applied to NF1 tumors. To this end, we will first determine whether NF1 heterozygosity alters the responsiveness of endothelial cells to angiogenic regulators. We will test if Nf1-/+ endothelial cells are particularly responsive to pro-angiogenic factors produced by NF1 tumor cells and, perhaps even more importantly, which anti-angiogenic factors are most effective in abrogating the angiogenic response evoked by NF1 tumors. In particular, endostatin will be thoroughly examined as a potential anti-angiogenic therapy for NF1 tumors. Gene therapy for NF1 tumors has not been tested due to the lack of an appropriate NF1 tumor model. We have established a working xenograft model of neurofibroma in the mouse in which the efficacy of endostatin gene therapy will be accessed. This model involves the initiation of neurofibromas by implantation of human NF1 tumor-derived, neurofibromin-null Schwann cells into the nerves of mice with an Nf1-/+ background. Tumor progression and vascularity will be assessed in vivo by MRI non-invasive imaging. MRI data will be corroborated by end-point histology using precise labeling of tumor and host cell components.

15. SUBJECT TERMS
cancer biology, angiogenesis, xenograft, gene therapy, anti-angiogenic therapy, MRI

16. SECURITY CLASSIFICATION OF:			**17. LIMITATION OF ABSTRACT**	**18. NUMBER OF PAGES**	**19a. NAME OF RESPONSIBLE PERSON**
a. REPORT	**b. ABSTRACT**	**c. THIS PAGE**			USAMRMC
U	U	U	UU	61	**19b. TELEPHONE NUMBER** *(include area code)*

Table of Contents

INTRODUCTION

Neurofibromatosis type 1 (NF1) is a common genetic disease with a wide variety of features which primarily involve the nervous system and related tissues. NF1 is characterized by abnormal cell growth and a high incidence of neurofibroma, a nerve tumor composed predominantly of Schwann cells. Plexiform neurofibromas often grow very large and are debilitating or fatal to NF1 patients. Thus, there is a serious need for better therapies to manage NF1 tumor growth. To this end, we have developed and exploited two animal models of NF1. The first involves a strain of mice in which the *Nf1* gene was functionally deleted. These Nf1 knockout mice are a valuable model for examining the biology of Nf1 tissues both in vivo and in vitro. Secondly, we have cultured tumor cells from human NF1 tumors. These human cell lines form neurofibroma-like tumors when implanted into the mouse nerve. Using these resources and animal models we can examine the formation of NF1 tumors under controlled conditions. The Aims of this proposal are to determine how NF1 tumors induce the formation of new blood vessels and to test therapies to inhibit this process as an means to stop tumor growth.

There is considerable heterogeneity in the vasculature found in different tissue and tumor types. The first Aim of this work is to determine whether blood vessel formation might be altered in NF1 patients. For this we will use the Nf1 knockout mouse. Endothelial cells will be cultured from wild-type and Nf1-/+ mouse tissues. The ability of these cells to form blood vessels in response to pro-angiogenic and anti-angiogenic factors will be tested in tissue culture assays. Important differences in the responsiveness of Nf1 endothelial cells will be confirmed using in vivo assays conducted in wild-type and Nf1 knockout mice.

We have established and characterized numerous cell cultures from human NF1 tumors, many of which have been grown as tumor grafts in the nerves of Nf1 mice. We will test the hypothesis that the rate of growth by these NF1 tumor xenografts is associated with the degree of newly formed vasculature. Also, comparisons will be made between xenografts implanted in normal mice and Nf1 mice. In vivo tumor growth and vascularity will be correlated with the expression of angiogenic regulators by the implanted cell lines. These experiments will test the hypothesis that tumor growth and invasion is dependent on the responsiveness of Nf1 endothelial cells and other reactive cells in the nerve that contribute to tumor formation.

There are several anti-angiogenic factors that show excellent promise as potent inhibitors tumor growth. In this aim we will test endostatin as an anti-tumor treatment for peripheral nerve tumors in NF1. This Aim will be expanded to include other anti-angiogenic therapies based on discoveries made in the Aims described above. Gene therapy using endogenous angiogenic inhibitors, like endostatin, is considered by many to be the most promising approach to bring the anti-angiogenic therapy into the clinic. As a simplified experimental model, we will examine the growth and vascularity of tumor xenografts that are engineered to produce endostatin. Second, using a strategy more relevant to clinic treatment, we will apply an endostatin-viral vector (AAV-endostatin) to NF1 tumors already growing in the mouse. In both treatment models, growth and regression of tumor and neovasculature will be monitored in vivo by non-invasive magnetic resonance imaging (MRI) followed by autopsy examination of the tumor tissues. Our overall goal is to discover effective therapies for the treatment of plexiform neurofibromas by blocking the ability of these aggressive tumors to recruit the blood vessels required for their growth.

BODY

Technical Objective 1: EXAMINE THE RESPONSE OF NF1 ENDOTHELIAL CELLS TO ANGIOGENIC REGULATORS.

Task 1: Perform in vitro assays of Nf1+/- endothelial cell responses to pro-angiogenic factors:

Progress: This Task was completed (see 2005 Annual Report). In addition, these findings have now been described in detail in a report published this year (Wu et al., 2006). Findings in our 2005 Annual Report involved the heightened response of Nf1+/- endothelial cells to pro-angiogenic factors in proliferation assays. We have now also tested the effects of these factors on endothelial cell migration in vitro. In brief, Nf1+/- and wild-type endothelial cells showed no significant differences in migratory responses to pro-angiogenic factors (as shown for VEGF in Fig. 1).

Task 2: Perform in vitro assays of Nf1+/- endothelial cell responses to anti-angiogenic factors:

Progress: This Task has been completed for our primary anti-angiogenic factor, endostatin. Nf1+/- and wild-type endothelial cells showed no significant differences in proliferation responses to endostatin (not shown). Next, we tested endothelial cell migration, another feature of ECs that is functionally important in angiogenesis. Cell migration was stimulated by VEGF in a Boyden chamber assay (which as stated above stimulated both endothelial cells of both genotypes equally). To asses the susceptibility of Nf1 haploinsufficient endothelial cells to angiogenic inhibitors, we then treated the stimulated cells with endostatin. Endostatin inhibited the migration of both genotypes and had a more pronounced effect on Nf1 haploinsufficient endothelial cells (Fig. 2). This indicates that Nf1 haploinsufficiency in endothelial cells may cause these cells to be more susceptible to the effects of this angiogenic inhibitor and provides a logical rationale for testing endostatin to inhibit tumor angiogenesis and negate tumors growth in NF1 patients. Although our testing provided consistent results, we are in the progress of performing additional experiments to confirm these findings and determine the maximal effects of endostatin on Nf1+/- endothelial cells .

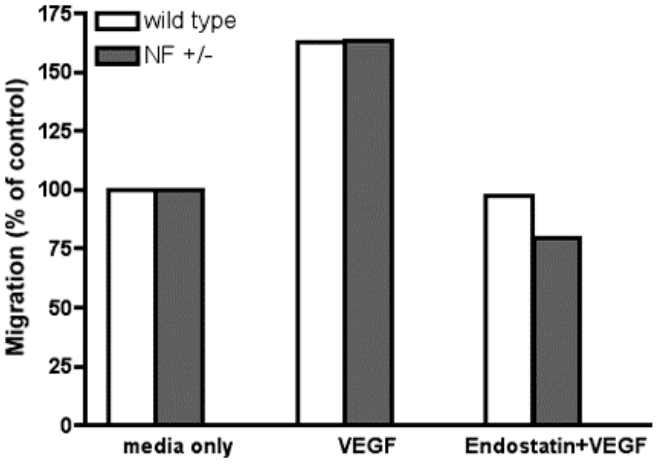

Figure 1. Increased sensitivity to endostatin by Nf +/- endothelial cells. Migration of brain microvessel endothelial cell cultures in a Boyden chamber assay. Nf1+/– and wild-type endothelial cell cultures were stimulated to migrate with a base medium only (control) or base medium containing VEGF. Endostatin (1 μg/ml) was added to the VEGF stimulated cultures. Data represent counts of migrating cells, expressed as a percentage of control.

Task 3: Perform in vivo assays for angiogenesis in Nf1+/- knockout mice:

Progress: This Task was completed (see 2005 Annual Report). In addition, these findings have now been described in detail in a report published this year (Wu et al., 2006).

Task 4: Determine the angiotrophic potential of human tumor cell lines:

Progress: For this Task we have collected extracts from numerous NF1 tumor cultures and normal Schwann cell control cultures. We have tested many of these to determine the proliferative and migratory responses of Nf1+/- endothelial cells to factors produced by NF1 tumor cultures. Thus far results have been varied and sometimes ambiguous. It is our belief that the tumor cultures produce both promoters and inhibitors of endothelial cell proliferation and migration. We conclude that the cultures have a balanced biological activity which, in most cases, is neither net promotive or inhibitory. Mainly, this Task has been completed. However, we are in the process of confirming our conclusion by performing a few key biochemical assays to demonstrate the culture samples indeed contain known pro- and anti-angiogenic factors. To this end, we have already found that all of our NF1 tumor cultures produce the endothelial cell mitogen VEGF and the antiangiogenic factor endostatin. The prevalence of these two antagonist might well explain the neutrality of these culture extracts in our in vitro assays.

Technical Objective 2: EXAMINE THE VASCULARITY AND ANGIOGENIC PROPERTIES OF NF1 TUMOR XENOGRAFTS.

Task 1: Develop MRI imaging of tumor growth and vascularity:

Progress: Our goal in this Task is to establish methods and parameters for MRI imaging of tumor growth and regression in a xenograft model of neurofibroma. Schwann cell cultures from NF1 patient tumors were implanted in the nerves of mice with an Nf1 background. The methods and characterizations of these tumors by histology and MRI were compiled into two manuscripts that have been submitted for publication (Perrin et al., 2006a, 2006b). We have established and imaged numerous xenografts using various MRI parameters including T1 and T2-weighting. Also, the vascular properties of tumor xenografts were imaged using gadolinium enhancement. Xenografted tumors appeared as hyperintense regions on *in vivo* T2-weighted MRI. Figure 2 shows T2-weighted images from a representative xenografted mouse over time. A slight hyperintensity is seen two weeks after xenograft of sNF96.2 cells at the site of tumor cell injection (Fig. 2A). By five weeks, the tumor is easily visible (Fig. 2B) and is shown to increased in size by week eight (Fig 2C). In this and other experiments, the hyperintense tumor regions were shown to increase in size as the tumor developed and grew over time and were subsequently verified as xenografted sNF96.2 cells by huGST immunostaining. ThusT2-weighted, *in vivo* MRI is a useful tool for use in monitoring tumor growth over time and can subsequently be used to test the effectiveness of therapeutic agents *in vivo*. We have made excellent progress in imaging tumor xenografts by MRI and are ready to apply these techniques to monitor tumor growth and, in particular, tumor regression in response to anti-angiogenic treatments as required for subsequent aims.

Figure 2.

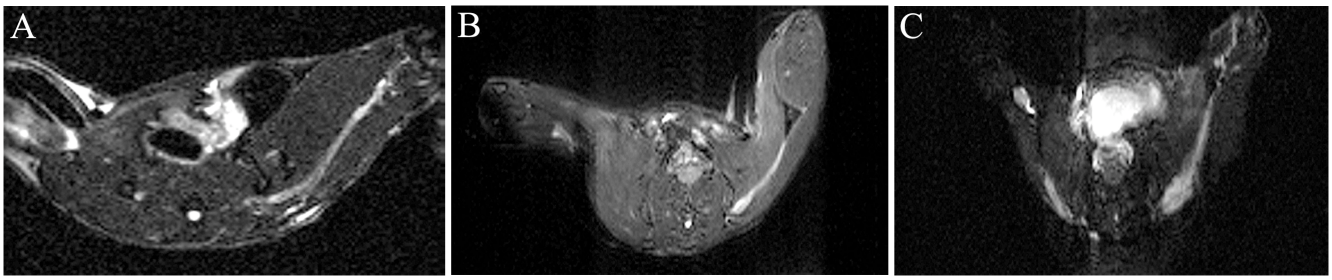

Task 2: Develop volumetric MRI and histology methods for tumor quantitation:

Progress: This Task is mainly completed, although we continue to improve our methods and applications for of volumetric quantitation of tumor growth by MRI and histology. As stated above, MRI imaging is now established and the data sets have been and continued to be studied by post-hoc image analysis. We made 3D renderings of many tumor image sets (from consecutive slices) and have performed volumetrics of tumor size. An example is provided in Figure 3 showing a subset of representative MRI slices (4 of 11 in which tumor was detected), tumor definition and volume calculations. In summary, we successfully applied MRI methods for in vivo tumor monitoring and these measurements correlate well with follow-up histology assessments. Although applying this to subtle aspects of tumor growth is an evolving skill, our methods are in place to assess tumor volume for conservative the quantitative scoring required in subsequent aims.

Figure 3.

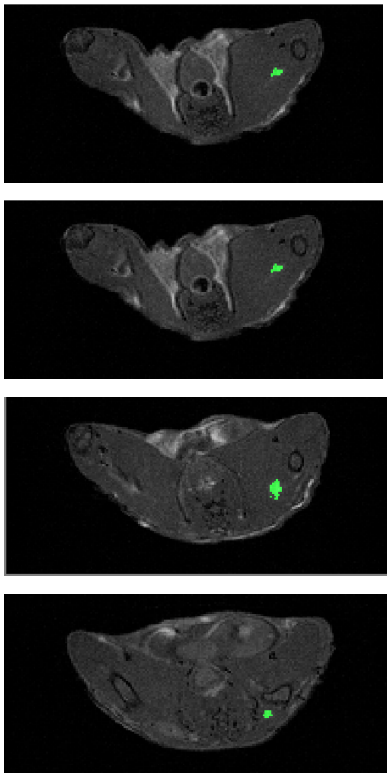

Slice	Volume (mm^3)
1	0.3689
2	0.4557
3	0.7812
4	0.7595
5	0.8898
6	0.5859
7	0.8680
8	0.6510
9	0.6944
10	0.3906
11	0.2821
Total	**6.7271**

Task 3: Quantify the growth and neovascularity of NF1 tumor xenografts:

Progress: This Task has mainly been completed although, like our other imaging and scoring efforts, we are making a continued effort to improve and refine image quality, discrimination and quantitation. Our goal is to analyze and compare the growth and vascularity of various xenografts with different growth properties. Vascularity assessed by in vivo gadolinium enhancement has been established and quantified. To demonstrate increased vascular permeability, an assessment of angiogenesis, dynamic contrast-enhanced magnetic resonance imaging (DCE-MRI) was also performed 8 weeks after xenograft. DCE-MRI showed a hyperintense region in the xenografted area of the nerve, shown later by human GST immunostaining to be xenografted tumor, while a contralateral, uninjected sciatic nerve showed only a slight rise in contrast intensity. Approximately 17 minutes after contrast injection, when

the level of contrast enhancement peaked, (Fig. 4), the xenografted tumor displayed an average contrast enhancement 7.9 fold higher than the surrounding muscle while the normal, uninjected nerve showed only an average 2.1 fold increase over the surrounding muscle over the next 15 minutes. These results suggest an increased vascular permeability in the xenografted tumor, which correlate with our histological findings of tumor-induced angiogenesis.

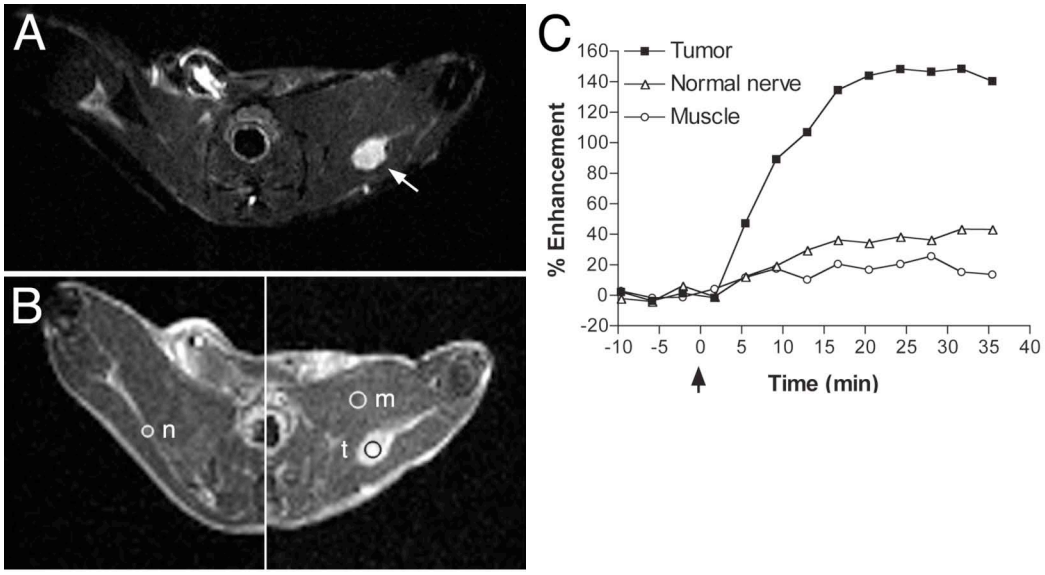

Figure 4. sNF96.2 xenograft tumor growth was monitored by i*n vivo* MRI. (A) T2-weighted MRI reveals a large tumor mass (arrow) 8 weeks after implantation. (B) T1 weighted, DCE-MRI from the same mouse shown in A after systemic injection of the contrast agent gadolinium: The left image shows the contralateral sciatic nerve, which was not injected with tumor cells. DCE-MRI shows increased tumor blood vessel permeability. (C) The graph shows the % enhancement in specified regions of interest (indicated by the circles; n, normal nerve; t, xenograft tumor; m, muscle) over time after injection of the contrast agent. This increase in % enhancement corresponds to increased vascular perfusion in xenografted tumor and tumor vascularity.

Task 4: Determine the effect of the Nf1+/- background on NF1 tumor xenografts:

Progress: This Task was completed (see 2005 Annual Report). In addition, these findings have now been included in two papers submitted for publication (Perrin et al., 2006a; 2006b).

Task 5: Examine the angiogenic properties of Nf1+/- host cells within the NF1 tumor xenograft:

Progress: In this aim we will examine the possible tumorigenic and angiotrophic contributions of other Nf1-/+ host cell types. We have examined the distribution of host mast cells associated with the xenografts. In brief, these reactive cells accumulate around all xenograft tumors and infiltrate certain xenograft types much more than others. These findings and possible implications are presented in two papers submitted for publication (Perrin et al., 2006a; 2006b). Next, we plan to examine mast cell association with neovascular elements at the tumor margins. We have not yet performed any immunocytochemical labeling to determine the expression of angiotrophic factors by reactive mast cells. In summary, this Task is partially complete and work is still ongoing.

Technical Objective 3: EXAMINE THE EFFECTS OF ANGIOGENIC INHIBITORS ON THE GROWTH AND NEOVASCULARIZATION OF NF1 TUMOR XENOGRAFTS IN NF1+/- MICE.

Task 1: Transduce endostatin in NF1 tumor cultures:

Progress: We have completed the transfection of one NF1 tumor cell line with AAV-endostatin. Work on the second is underway. Transfection efficiency in the NF1 tumor cell lines is low and requires subcloning and selection for stably transfected, highly productive clones. This effort has been very slow and difficult because the cell lines do not grow well from single cells. Thus far we have characterized several subclones and identified one acceptable for use in follow-up experiments.

Task 2: Determine the effect of endostatin in vitro transduction on NF1 tumor xenografts:

Progress: This aim has been partially completed. Thus far we have performed the in vitro assay to determine if endostatin effects the proliferation and migration and migration of the NF1 tumor cell lines. Testing is complete on the cell lines that we have focused on for xenografting and results show endostatin does not effect their tumorigenic properties. These tests are mostly confirmatory. It would have been therapeutically useful if this anti-angiogenic factor inhibited growth by NF1 tumor cells in addition to vascular endothelial cells. On the other hand, if this was true it would have been difficult for us to assess the antiangiogenic effects of endostatin per se. The second approach to this question involves examining the growth of NF1 tumor cell transfected with endostatin as xenografts in vivo. These tests were somewhat delayed because of difficulties in transfection and subcloning. Nevertheless, our first set of animals have been engrafted with endostatin transfected NF1 tumors and a second set is scheduled. This effort also involved establishing assays to measure endostatin production by these tumors, for which we have developed an accurate ELISA for testing human endostatin in blood samples taken from engrafted mice. Tumor progression in these animals will be monitored by in vivo MRI, as described in previous Tasks.

Task 3: Develop in vivo delivery of AAV-endostatin:

Progress: We have tested several methods for in vivo delivery of endostatin. Based on recent reports, to achieve significant tumor control high doses of endostatin must be injected at least daily. This is a very expensive protocol. Furthermore, the same studies show that endostatin is most effective when blood levels are maintained. We anticipated this dosing regime and therefore we proposed intramuscular injection of AAV-endostatin for constant production. Thus far, we have made several attempts at intramuscular transduction but have failed to achieve significant endostatin levels in the mouse blood. Additional experiments are underway using larger AAV-injections. It is essential that we test the effects of systemic endostatin on the growth of established tumors. Therefore we have tested an alternative method. In our initial testing of the transfection efficiency of AAV-endostatin we infected 293 cells, commonly used for this purpose because of their known high transduction efficiency. We found that when injected subcutaneously in our host mouse strain these cells form slow growing tumors and secrete high levels of endostatin into the blood stream. We are presently finalizing methods to consistently establish these endostatin factories and will soon use this approach to treat NF1 tumor xenografts in the mouse nerves.

Task 4: Assess the effect of endostatin delivery to established NF1 tumor xenografts:

Progress: As described above, we have characterized two NF1 tumor xenograft models. Methods are in place to monitor tumor growth and tumor vascular perfusion in vivo by MRI. Also, a method of constant endostatin delivery implantation of endostatin transfected 293 cells has been developed. And, assays are

in place to monitor endostatin levels in the blood of mice with NF1 tumor xenografts. At this time we are only waiting for the mice to serve as hosts in these experiments. We have been breeding scid mice with an Nf1+/- background for several years. This cross-bred strain is essential to our xenografting experiments. Over the past year the success rate of our colony has diminished and we recently started back-cross matings to establish more productive breeders. This problem may be associated with the scid strain (not the Nf1 strain) because our mouse supplier has been experiencing similar breeding problems. This incurred additional delays because of their backcrossing efforts and subsequent backlog of orders. With that behind us, it now seems our colony is recovering and we anticipate an adequate supply of scid/Nf1+/- mice in the near future.

KEY RESEARCH ACCOMPLISHMENTS

1) Developed methods to culture brain microvessel endothelial cells from Nf1 and wild-type mice.
2) Found that Nf1+/- endothelial cells have an exaggerated proliferative response to pro-angiogenic factors in vitro and in vivo.
3) Found that endostatin is a potent inhibitor of certain angiogenic properties of Nf1+/- endothelial cells in vitro.
4) Established and documented valid xenograft models of NF1 plexiform neurofibroma and malignant peripheral nerve sheath tumors.
5) Quantified tumor growth and vascularity of NF1 tumor xenografts.
6) Imaged and quantified vascularity of xenografted tumors using MRI, gadolinium permeability and dynamic contrast enhancement.
7) Established and subcloned NF1 tumor line transfected with AAV-endostatin.
8) Developed experimental delivery system for endostatin by establishing subcutaneous “cell factory” using 293/AAV-endostatin cell line.

REPORTABLE OUTCOMES

Manuscripts:

M. Wu, M.R. Wallace, **D. Muir**. 2005. Tumorigenic properties of neurofibromin-deficient Schwann cells in culture and as syngrafts in *Nf1* knockout mice. Journal of Neuroscience Research 82: 357-367.

M. Wu, M.R. Wallace, **D. Muir**. 2006. Nf1 haploinsufficiency augments angiogenesis. Oncogene 25: 2297-2303.

L. Fishbein, X. Zhang, L.B. Fisher, H. Li, M. Campbell-Thompson, A. Yachnis, A. Rubenstein, **D. Muir**, M.R. Wallace. 2006. In vitro studies of steroid hormones in Neurofibromatosis 1 tumors and Schwann cells. Molecular Carcinogenesis (in press)

G.Q. Perrin, L. Fishbein, S.A. Thomson, M.S. Hwang, M.T. Scarborough, A.T. Yachnis, M.R. Wallace, T.H. Mareci, **D. Muir**. Malignant peripheral nerve sheath tumors developed in the mouse by xenograft of an NF1 tumor-derived Schwann cell line. (submitted)

G.Q. Perrin, L. Fishbein, S.A. Thomson, K. Stephens, J. Garbern, A.T. Yachnis, M.R. Wallace **D. Muir**. Plexiform neurofibromas developed in the Mouse by xenograft of an NF1 tumor-derived Schwann cell line. (submitted)

Abstracts:

G. Perrin, M. Wallace and D. Muir. 2005. Characterization of two reproducible xenograft models for NF1 tumors. National Neurofibromatosis Foundation Meeting, Aspen, CO.

Animal Resources: None

CONCLUSIONS

Work on this research project has been conducted in a timely fashion with very good progress. In vivo and in vitro models were used to firmly conclude that Nf1 haploinsufficiency in endothelial cells results in exaggerated proliferation and angiogenesis to key pro-angiogenic factors. These results implicate these growth factor pathways as potential targets for therapeutic agents. In addition, we found that endostatin is a potent inhibitor of Nf1+/- endothelial cell migration in vitro. This suggests that endostatin may be a particularly effective therapy for reducing tumor NF1 tumor growth by inhibiting the formation of new blood supply.

We have made excellent progress in aims to establish reliable procedures for xenografting of human NF1 cell lines in the mouse. Thus, far, we established and documented two valid xenograft models of NF1 peripheral nerve sheath tumors. Using these models, tumor growth and vascularity of NF1 tumor xenografts has been quantified by advanced MRI, gadolinium permeability and dynamic contrast enhancement that match results obtained by conventional histological measurements.

In summary, the work and aims of this project are mainly proceeding on schedule. Definitive findings were made in the in vivo models of neovascularization and MRI assessment of tumor growth and vascularity. Work on other aims is progressing well. Several reports were published that detail these findings and two others have been submitted for publication.

REFERENCES

M. Wu, M.R. Wallace, **D. Muir**. 2005. Tumorigenic properties of neurofibromin-deficient Schwann cells in culture and as syngrafts in *Nf1* knockout mice. Journal of Neuroscience Research 82: 357-367.

M. Wu, M.R. Wallace, **D. Muir**. 2006. Nf1 haploinsufficiency augments angiogenesis. Oncogene 25: 2297-2303.

G.Q. Perrin, L. Fishbein, S.A. Thomson, K. Stephens, J. Garbern, A.T. Yachnis, M.R. Wallace **D. Muir**. 2006a. Plexiform neurofibromas developed in the Mouse by xenograft of an NF1 tumor-derived Schwann cell line. (submitted)

G.Q. Perrin, L. Fishbein, S.A. Thomson, M.S. Hwang, M.T. Scarborough, A.T. Yachnis, M.R. Wallace, T.H. Mareci, **D. Muir**. 2006b. Malignant peripheral nerve sheath tumors developed in the mouse by xenograft of an NF1 tumor-derived Schwann cell line. (submitted)

APPENDICES

3 reprints

Journal of Neuroscience Research 82:357–367 (2005)

Tumorigenic Properties of Neurofibromin-Deficient Schwann Cells in Culture and as Syngrafts in *Nf1* Knockout Mice

Min Wu,[1] Margaret R. Wallace,[2,3] and David Muir[1,3]

[1]Department of Pediatrics, Division of Neurology, University of Florida College of Medicine, Gainesville, Florida
[2]Department of Molecular Genetics and Microbiology, University of Florida College of Medicine, Gainesville, Florida
[3]McKnight Brain Institute and Shands Cancer Center, University of Florida College of Medicine, Gainesville, Florida

Neurofibromatosis type 1 (NF1) is one of the most common dominantly inherited genetic diseases associated with the nervous system. Functional loss of the *NF1* tumor suppressor is frequently associated with the generation of benign neurofibromas that can progress to malignancy. Recent evidence in genetic mouse models indicates that the development of neurofibromas requires a loss of *Nf1* in the cells destined to become neoplastic as well as heterozygosity in nonneoplastic cells. We tested this hypothesis in a newly developed syngraft mouse model in which $Nf1^{-/-}$ Schwann cells isolated from knockout embryos were grafted into the sciatic nerves of $Nf1^{+/-}$ mice, corresponding to the genetic background of NF1 patients. Furthermore, we also characterized in vitro growth of these cells. We found that embryonic mouse $Nf1^{-/-}$ Schwann cells exhibit increased proliferation and less growth factor-dependence in vitro compared with heterozygous and wild-type counterparts. Moreover, $Nf1^{-/-}$ Schwann cells showed tumorigenic growth when implanted into nerve of adult *Nf1* heterozygous mice. These findings support the conclusion that loss of *Nf1* in embryonic mouse Schwann cells is sufficient for tumor development in the heterozygous environment of adult mouse nerve. In addition, this syngraft model provides a practical means for the controlled induction of neurofibromas, greatly facilitating localized application of therapeutic agents and gene delivery.

Key words: neurofibromatosis type-1; neurofibroma; *Nf1* knockout; Schwann cell; gene transfer; tumor model

Neurofibromatosis type 1 (NF1) is one of the most common autosomal dominant genetic diseases, found in 1/3,500 individuals (Riccardi, 1992). Functional loss of the *NF1* tumor suppressor is frequently associated with the generation of benign neurofibromas. Neurofibromas show marked cellular heterogeneity, including Schwann cells, fibroblasts, and perineural, endothelial, and mast cells (Erlandson and Woodruff, 1982; Peltonen et al., 1988). The plexiform neurofibroma, a large Schwann cell tumor usually associated with primary nerves, can physically impede normal neurological functions and may progress to the malignant peripheral nerve sheath tumor, the most common malignancy associated with NF1 (Korf, 1999). Because plexiform neurofibromas are not discrete masses, surgical removal (the only clinical approach) is rarely complete, and recurrence is frequently associated with increased morbidity and mortality.

NF1 is caused by disruptive mutations in the *NF1* gene, which encodes neurofibromin, a protein that harbors a functional Ras-GAP (guanosine triphosphatase-activating protein) domain in its central region (Ballester et al., 1990; Xu et al., 1990). Because *NF1* is a tumor suppressor gene, it was predicted that a somatic disruption of the remaining *NF1* allele is a major determinant in neurofibroma formation. Indeed, there are several reports of disruption of both *NF1* alleles in neurofibromas (see, e.g., Colman et al., 1995; Rasmussen et al., 2000; Upadhyaya et al., 2004). The examination of cellular expression of neurofibromin in tumors and derivative cultures shows that most neurofibromas contain populations of neurofibromin-negative and neurofibromin-positive Schwann cells (Serra et al., 2000; Muir et al., 2001; Rutkowski et al., 2000), consistent with the two-hit hypothesis (Knudson, 2000). In addition, neurofibromin-deficient Schwann cells derived from NF1 tumors show a growth advantage in vitro and induced hyperplastic lesions that resemble plexiform neurofibroma in a xenograft mouse model (Muir et al., 2001). Although it is clear that loss of *NF1* in Schwann cells is associated with neoplasia in NF1, recent evidence suggests that heterozygosity (haploinsufficiency) in nonneoplastic cells is

Correspondence to: David Muir, Department of Pediatrics, Neurology Division, Box 100296, JHMHC, University of Florida College of Medicine, Gainesville, FL 32610. E-mail: muir@ufbi.ufl.edu

Received 21 March 2005; Revised 28 June 2005; Accepted 4 August 2005

Published online 22 September 2005 in Wiley InterScience (www.interscience.wiley.com). DOI: 10.1002/jnr.20646

also required for the complete *NF1*-mediated tumorigenicity (Zhu et al., 2002).

In *Nf1* knockout mouse strains, homozygous mutant mice die in utero by day 13 as a result of abnormal cardiac development (Brannan et al., 1994; Jacks et al., 1994). Heterozygous *Nf1* mice do not develop neurofibromas, indicating that loss of both *Nf1* alleles is essential for neurofibroma formation. Chimeric mice harboring both $Nf1^{-/-}$ and $Nf1^{+/+}$ cells develop plexiform neurofibromas derived exclusively from the $Nf1^{-/-}$ cells (Cichowski et al., 1999). These studies were unable to identify the specific cell type(s) responsible for tumor initiation. By using a conditional (*cre/lox*) allele, Zhu and coworkers (2002) found that *Nf1*-mediated tumorigenicity requires a loss of *Nf1* in Schwann cells as well as haploinsufficiency in nonneoplastic cells. In both models, tumors appear sporadically in unpredictable sites, which may limit their application for testing antitumor therapies using local treatment. In addition, genetically engineered mice that create fields of mutant $Nf1^{-/-}$ cells might not recapitulate all the microenvironment alterations required for the clonal outgrowth of human *NF1* tumors.

In the present study, a syngraft mouse model was developed to test the hypothesis that $Nf1^{-/-}$ Schwann cells initiate neurofibroma formation under spatial and temporal control. $Nf1^{-/-}$ Schwann cells were cultured from E12.5 $Nf1^{-/-}$ mouse embryos and implanted into the sciatic nerves of adult mice with an $Nf1^{+/-}$ background. We found that $Nf1^{-/-}$ Schwann cells have a growth advantage both in vitro and in vivo, producing tumors resembling plexiform neurofibroma in the adult haploinsufficient mouse nerve.

MATERIALS AND METHODS

Mouse Breeding

Mouse embryos were derived from two related colonies of *Nf1* knockout mouse strains. Inbred embryos were obtained from our stock colony of *Nf1* knockout mutant mice with the C57BL/6 background (B6/*Nf1*; Brannan et al., 1994). Other embryos were obtained by crossing B6/*Nf1* heterozygous females with *Nf1* heterozygous male mice on the 129/Sv background (129/*Nf1*; Brannan et al., 1994). Host mice with an *Nf1* mutation that were also immunodeficient were generated by crossbreeding B6/*Nf1* and B6/*scid* mice (*scid*/*Nf1*). Mice with $scid^{-/-}$/$Nf1^{+/-}$ genotype (designated *scid*/$Nf1^{+/-}$) were selected as hosts by genotype screening. The original *scid* mice were obtained from the Jackson Laboratory (Bar Harbor, ME). This project was reviewed and approved by the institutional Animal Care and Use Committee.

Genotyping

The *Nf1* locus was genotyped by a 3-oligo system PCR, as described by Brannan et al. (1994). The *scid* mutation in the DNA-PKCS gene, a nonsense mutation, was described by Blunt et al. (1996). We developed a PCR-based genotype assay based on genomic DNA sequence (Genbank AB005213). PCR primers were designed flanking the mutation site in exon 85: *scid* 5′ (GAGTTTTGAGCAGACAATGCTGA) and *scid* 3′ (CTTTTGAACACACACTGATTCTGC). The resulting 180-bp PCR product was digested with Alu I to distinguish wild-type allele (no cut) from mutant allele (cut) via agarose gel electrophoresis, to genotype animals at the *scid* locus.

Embryonic Schwann Cell Culture

Approximately 50 dorsal root ganglia (DRG) and attached nerve roots were removed from each embryo at E12.5. The tissue was dissociated for 1 hr at 37°C in Dulbecco's modified Eagle's medium (DMEM) containing collagenase (0.5 mg/ml, 1,200 U/mg) and dispase (5 U/ml). The digested tissue was dispersed by triturating 10–15 times with a flame-constricted, siliconized Pasteur pipette. One half of dispersed cells from each embryo were plated into one well of a six-well plastic culture plate, precoated with polyornithine (0.1 mg/ml) and then laminin (10 μg/ml; Muir, 1994). The cultures were grown in 0.5 ml of DMEM supplemented with 2% fetal bovine serum (FBS), antibiotics, β-nerve growth factor (NGF; 25 ng/ml; Becton Dickinson, Bedford, MA), human recombinant glial growth factor-2 (GGF2; 10 ng/ml; Cambridge Neuroscience, Cambridge, MA), and human recombinant fibroblast growth factor-2 (FGF2; 10 ng/ml; Becton Dickinson). After 10 hr of incubation at 37°C in 5% CO_2/humidified air, the medium was topped off with 1.5 ml of the same medium, except that the serum was replaced with N2 supplements and 1% heat-treated bovine serum albumin. After 3 days, the culture medium was refreshed with the serum-free medium describe above, with the exclusion of NGF. After 7–8 days, the culture was dissociated by brief trypsinization, and the Schwann cell-enriched cultures were pooled with others of the same genotype and seeded at a density of 2×10^6 cells/75 cm^2 in laminin-coated dishes in DMEM containing 2% FBS and GGF2 (10 ng/ml). These Schwann cell-enriched cultures (designated *P0*) were grown for at least 7 days and then used for in vitro and in vivo characterizations.

In Vitro Schwann Cell Proliferation Assay

Embryonic Schwann cell cultures were plated on laminin-coated, eight-chamber glass slides at 20,000 cells/well in DMEM containing 2% FBS. Two days after plating, the medium was changed to include treatments as indicated with the addition of bromodeoxyuridine (BrdU; 10 μg/ml). After 24 hr, the cultures were fixed with 2% paraformaldehyde. Percentages of cells with BrdU-positive DNA were scored by immunostaining as described previously (Muir et al., 1990).

In Vitro Schwann Cell Apoptosis Assay

Schwann cells were plated and grown as described for the proliferation assays. After 24 hr, cells were fixed in 2% paraformaldehyde, and apoptotic cells were identified by using the in situ Apoptosis Detection Kit (Serologicals Corp., Norcross, GA; a TUNEL assay), following the protocol provided.

Prelabeling Schwann Cell Cultures with GFP-rAAV Gene Transfer

We used an adeno-associated virus (AAV) subtype 2 vector carrying a green fluorescence protein (GFP) marker gene

under a cytomegalovirus (CMV) enhancer and chicken β-actin hybrid (CMB) promoter, obtained from the University of Florida Gene Therapy Center Vector Core Lab. This marker gene transfer was needed to distinguish host from syngraft cells. Mouse embryonic Schwann cell cultures at P0 and P1 were harvested, washed with medium, and incubated with this vector (rAAV-GFP) at various MOI for 1 hr at 37°C. The cells were then plated on laminin-coated 35-mm dishes and in 0.5 ml of DMEM containing 2% FBS and GGF2 (10 μg/ml). After 4 hr, 1.5 ml of the same medium was added to the dishes; the medium was changed every 3–4 days. To assess any side effects of rAAV-GFP transduction on cell proliferation, transduced Schwann cells were plated on eight-chamber slides and processed as describe above for the bromodeoxyuridine (BrdU) incorporation assay. GFP expression was examined by immunofluorescence microscopy.

Intraneural Implantation of *Nf1* Knockout Schwann Cells

Mouse embryonic Schwann cell cultures transduced with rAAV-GFP with greater than 90% GFP expression efficiency were implanted into the nerves of $Nf1^{+/+}$and *scid*/$Nf1^{+/-}$ host mice. Dissociated cells were collected, rinsed thoroughly, and resuspended as dense slurry (10^8/ml) in Hank's balance salt solution. Young adult mice (2–3 months old) were anesthetized, and the sciatic nerves of both legs were exposed at midthigh. The cell suspension (5 μl, 5×10^5 cells) was incrementally injected within the nerve by using a fine needle (200 μm diameter) and syringe driven by a UMP-II micropump (World Precision Instruments, Sarasota, FL) mounted on a micromanipulator. The site was closed in layers with sutures and the revived mouse returned to specific pathogen-free housing. To assess in vivo proliferation, mice were given an IP injection of BrdU (150 μl, 10 mg/ml) 24 hr before harvesting the nerves. At various times after implantation, the animals were killed under anesthesia, and the nerves were removed and then fixed by immersion in 4% buffered paraformaldehyde. Nerve segments were embedded in paraffin and sectioned at 7 μm for immunohistochemical staining.

Immunohistochemistry

Schwann Cell Cultures. Monolayer cultures were immunophenotyped with antibodies to the Schwann cell antigens S-100 (Dako, Carpinteria, CA), the low-affinity nerve growth factor receptor (p75; hybridoma 200-3-G6-4; American Tissue Culture Collection, Rockville, MD), and growth-associated protein-43 (GAP-43; NB300-143; Novus Biological, Littleton, CO; Ferguson and Muir, 2000). Cultures grown on laminin-coated chamber slides were fixed with 2% paraformaldehyde in 0.1 M phosphate buffer (pH 7.2; PBS) for 20 min and then washed with PBS containing 0.5% Triton X-100. Nonspecific antibody binding was blocked with PBS containing 0.1% Triton and 10% normal serum (blocking buffer) for 1 hour. Primary antibodies were diluted in blocking buffer and applied to wells overnight at 4°C. Bound antibodies were detected with fluorescein isothiocyanate (FITC)-conjugated secondary antibodies or peroxidase-conjugated secondary antibodies for 1 hr at 37°C. Peroxidase chromogenic development was accomplished with 3,3′-diaminobenzidine-$(HCl)_4$ (0.05%) and hydrogen peroxide (0.03%) in PBS.

Nerve Grafts. Sciatic nerves engrafted with mouse Schwann cells were fixed by immersion in 4% paraformaldehyde in PBS, sectioned longitudinally, and stained with hematoxylin and eosin (H&E) for routine light microscopic examination. To identify transplanted mouse Schwann cells, nerve sections were immunostained with polyclonal anti-GFP antibody (Molecular Probes, Eugene, OR). Deparaffinized sections were pretreated with methanol containing 1% hydrogen peroxide for 30 min to quench endogenous peroxidase activity. Nonspecific antibody binding was blocked with 10% normal serum in PBS containing 0.5% Triton X-100 for 30 min at room temperature. Primary antibodies were diluted in blocking buffer (1:500) and applied to sections overnight at 4°C. Bound antibodies were labeled with biotinylated secondary antibodies for 1 hr at 37°C, followed by the avidin-biotin-peroxidase reagent (Dako) for 2 hr. Chromogenic development was accomplished with 3,3′-diaminobenzidine-$(HCl)_4$ (0.05%) and hydrogen peroxide (0.03%) in PBS. A similar procedure was used for immunostaining with antibodies against von Willebrand's factor (1:500; Dako), anti-VEGF-R2/Flk-1 (1:100; Santa Cruz Biotechnology, Santa Cruz, CA), and anti-neurofilament (1:300; Sigma, St. Louis, MO). For all immunohistochemical stains, sections without addition of primary antibodies served as negative controls.

Cell proliferation within the engrafted nerves was assessed by systemic injection of BrdU. Engrafted nerves were sectioned on the longitudinal axis and immunostained for BrdU DNA as described previously (Muir et al., 1996). BrdU-positive nuclei were counted per high-power field under the microscope. Mast cells were identified by the Leder stain, a histochemical method for chloracetate esterase activity using Naphthol AS-D (3-hydroxy-2-naphoic acid-O-toluidine; Sigma).

RESULTS

Breeding *Nf1* Knockout Mice for Schwann Cell Cultures

Heterozygous *Nf1* mutant mice do not exhibit gross abnormalities, whereas homozygous mutant embryos die in utero by E13.5. By E12.5, the peripheral ganglia have formed sufficiently for the culture of Schwann cells from $Nf1^{-/-}$ embryos prior to death (Kim et al., 1995; Dong et al., 1999). From initial generations of breeding dams, live $Nf1^{-/-}$ embryos were readily obtained at day E12.5, averaging 15% of the offspring per litter (Brannan et al., 1994). However, protracted breeding of the original B6/$Nf1^{+/-}$ strain caused earlier mortality of $Nf1^{-/-}$ embryos in utero. At the beginning of this study, from 63 embryos derived from nine liters, we obtained only two live $Nf1^{-/-}$ embryos (a 3.2% surviving rate) at day E12.5. To overcome this shift toward earlier mortality, the B6/$Nf1^{+/-}$ mice were crossed with a 129/$Nf1^{+/-}$ strain. As a result, the surviving rate of $Nf1^{-/-}$ embryos at day E12.5 derived from B6/$Nf1^{+/-}$ females mated with 129/$Nf1^{+/-}$ males increased to 23.7% (approximating the expected Mendelian ratio). Thirty-one live $Nf1^{-/-}$ embryos were obtained from a total of 131 hybrid embryos in 16 litters. This

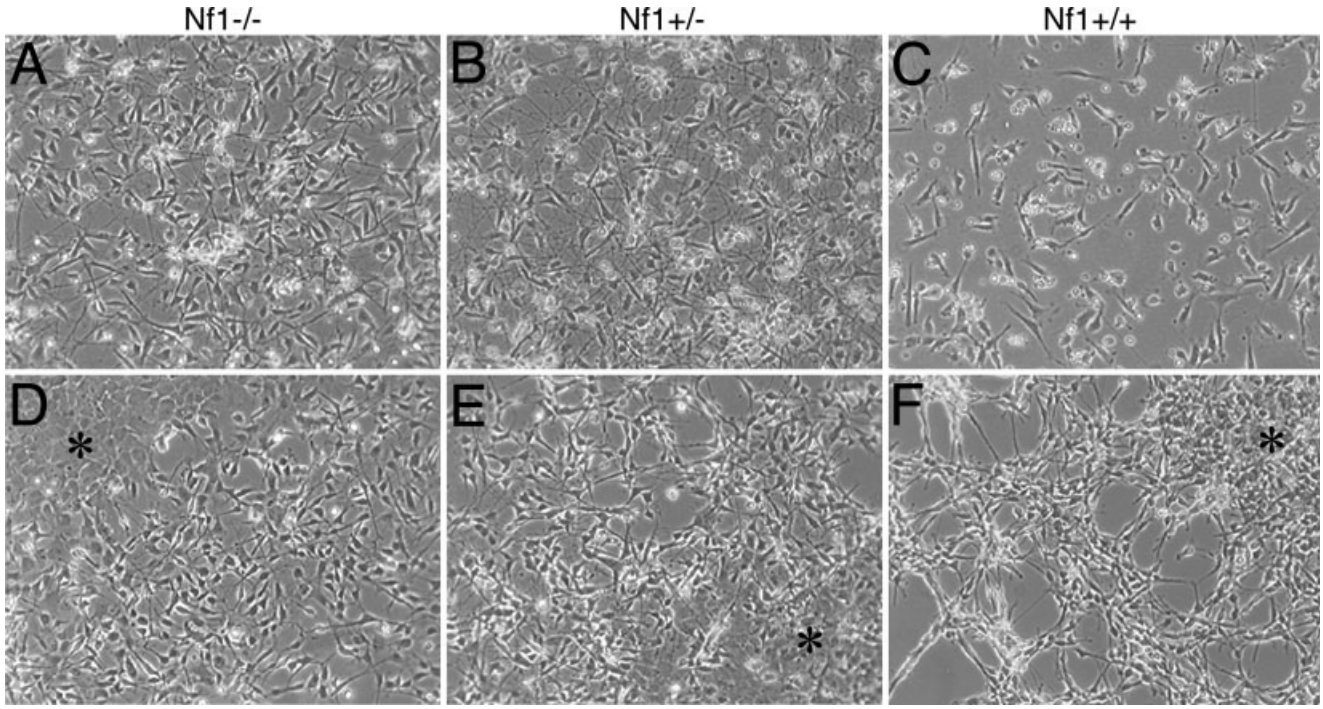

Fig. 1. Culture of embryonic *Nf1* knockout Schwann cells. Phase-contrast micrographs were taken from $Nf1^{-/-}$ (**A,D**), $Nf1^{+/-}$ (**B,E**), and $Nf1^{+/+}$ (**C,F**) embryo-derived Schwann cell cultures grown in low serum medium. A–C: At 2 days in vitro, Schwann cells initiated as bipolar or polygonal flatten cells. D–F: After 6 days, Schwann cells grow independently of axons in these cocultures and mainly appeared as phase-bright, spindle-shaped cells (SSC). Meanwhile, flat Schwann cell (FSC) colonies (asterisks) appeared in cultures of all three genotypes. Original magnification ×200.

cross-strain breeding improved the yield of $Nf1^{-/-}$ embryos obtainable at day E12.5 by more than sevenfold. The results described below involved the use of Schwann cells cultured from the B6/*Nf1* × 129/*Nf1* hybrid embryos.

Growth Characteristics and Phenotype of Cultured $Nf1^{-/-}$ Schwann Cells

Cultured Schwann cells with $Nf1^{-/-}$, $Nf1^{+/-}$, and $Nf1^{+/+}$ genotypes eventually developed unique phenotypes. At initial stages, Schwann cells of all three genotypes had a similar appearance, containing mostly bipolar, triangle, or polygonal flattened shapes, with limited elongation (Fig. 1A–C). After 1 week of culture, most Schwann cells from all three genotypes grew without close contact with axons and became more elongated, bipolar, and spindle-shaped Schwann cell (SSC; Fig. 1D–F), similar to the $Nf1^{-/-}$ Schwann cell described by Kim et al. (1995). Also, before the first passage, small colonies of flattened Schwann cells (FSC), like the reported TXF2/2 Schwann cells (Kim et al., 1997), started to appear in cultures of all three genotypes (Fig. 1D–F). Increased numbers of these colonies were often found in areas with high cell density regardless of genotype, indicating that they were more closely correlated with cell density than with genotype. The expansion of the FSC markedly increased as cultures approached confluence, suggesting that their proliferation was stimulated by autocrine factors or cell–cell contact.

After passage, the $Nf1^{-/-}$ cultures expanded more rapidly and had a higher ratio of FSC to SSC than the $Nf1^{+/-}$ or $Nf1^{+/+}$ cultures. In all cases, Schwann cell cultures rapidly stagnated and became senescent beyond passage 2 for $Nf1^{+/+}$ Schwann cell cultures, passage 4 for $Nf1^{-/-}$ cultures, and in between for $Nf1^{+/-}$ cultures. Immunostaining of these cells before passage 2 showed that at least 95% of cells were immunopositive for the Schwann cell markers S-100, p75, and GAP-43 (data not shown). These results indicate that most cultured cells in all three genotypes are of Schwann cell lineage and that the transformed FSCs are Schwann cell derivatives as well. Less than 5% of cells showed only nuclear staining with S-100, confirming that fibroblast contamination was low.

Growth Advantage of $Nf1^{-/-}$ Schwann Cells In Vitro

Although the growth properties of Schwann cell cultures varied in magnitude somewhat from litter to litter, differences observed among the three genotypes within littermates remained consistent. Cell counting of four different batches of initial cultures (each batch prepared from embryonic littermate embryos with genotypes

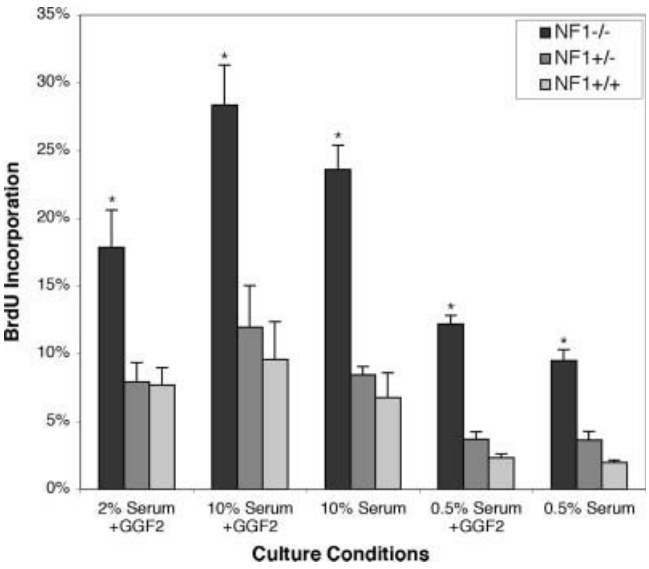

Fig. 2. Proliferation of Schwann cells derived from *Nf1* mutant and wild-type mouse embryos. Mouse Schwann cells cultured from $Nf1^{-/-}$, $Nf1^{+/-}$, and $Nf1^{+/+}$ embryos from the same litter at P0 were seeded onto laminin-coated chamber slides and grown in DMEM with 2% FBS for 48 hr, with an additional 24 hr of culture in replaced medium containing BrdU and indicated serum and GGF2, and cells were immunostained for BrdU and Hoechst. The percentages of BrdU-positive nuclei were obtained from the total number of Hoechst-stained nuclei. Data represent the mean (+SE) of triplicate assays for each culture condition and two replicate experiments. *Significant difference between mutant and wild-type genotypes (ANOVA, $P < 0.05$).

of $Nf1^{-/-}$, $Nf1^{+/-}$, $Nf1^{+/+}$) showed that the mean numbers of cells from these Schwann cell cultures were $Nf1^{-/-}$ 2.5 million (±0.28), $Nf1^{+/-}$ 1.6 million (±0.19), and $Nf1^{+/+}$ 1.0 million (±0.18). Differences between genotypes were statistically significant (*t*-test, $P < 0.05$). These results suggest that $Nf1^{-/-}$ Schwann cells and, to a lesser extent, $Nf1^{+/-}$ Schwann cells, have a significant growth advantage in vitro. Although it was evident that $Nf1^{-/-}$ Schwann cells cultures expanded more rapidly, it remains possible in this rudimentary analysis that cell numbers from the initial dissections differed significantly for each genotype. Therefore, we examined directly the effect of *Nf1* mutation on Schwann cell proliferation and apoptosis. Schwann cells of all three genotypes derived from littermates were cultured under the same conditions and were seeded at the same time for proliferation and apoptosis assays. BrdU incorporation assays revealed that proliferation of $Nf1^{-/-}$ Schwann cell cultures was markedly greater than that of heterozygous or wild-type cultures. This was true for various culture conditions tested (Fig. 2). When cells were grown in the presence of high serum or GGF-2, proliferation of $Nf1^{-/-}$ Schwann cells was two- to threefold greater than that of wild-type or $Nf1^{+/-}$ Schwann cells. In low-serum medium, proliferation by $Nf1^{-/-}$ cultures was nearly fivefold greater than that by wild-type or $Nf1^{+/-}$ Schwann cells, indicating that the $Nf1^{-/-}$ cells were less growth factor dependent. Similar results showing that $Nf1^{-/-}$ Schwann cells have a growth advantage in vitro were obtained from cultures at two different early passages as well (data not shown).

Because the majority of BrdU-positive Schwann cells were FSCs, poorly differentiated Schwann cells accounted heavily for the differences in proliferation observed between genotypes. However, proliferation by SSCs, assessed by scoring the percentage of BrdU-positive cells in the spindle-shaped cell population only, was at least twofold higher in the $Nf1^{-/-}$ cultures than in wild-type cultures. These findings confirm that $Nf1^{-/-}$ Schwann cells, both the SSC and the FSC morphological types, have a marked growth advantage in vitro. Thus, the growth advantage of $Nf1^{-/-}$ Schwann cells in vitro is attributed mainly to *Nf1* deficiency rather than culture heterogeneity or cell transformation per se.

TUNEL assays for apoptosis showed no significant differences in cell death between mutant and wild-type Schwann cells (data not shown). Therefore, the growth advantage of $Nf1^{-/-}$ Schwann cells compared with wild-type cells is due primarily to increased proliferation.

Prelabeling of Mouse *Nf1* Schwann Cell Cultures Using AAV Vector-Mediated Gene Transfer

Our next goal was to examine the growth of *Nf1* Schwann cell cultures as transplants in the nerves of mouse hosts. To prelabel the cells for implantation, Schwann cells of all three genotypes were transduced with rAAV-GFP vectors individually. With MOI > 1000, GFP expression was observed from most cells of all genotypes tested (Fig. 3A), up to 95% of cells in cultures of all three genotypes. Such GFP expression may remain strong for up to 30 days in vitro, although slight reduction was observed over time resulting from cell proliferation, because rAAV vectors generally persist as episomes in transduced cells and can be lost from dividing cells. Possible effects of vector transduction on Schwann cell characteristics (including morphology, marker gene expression, and cell proliferation) were examined after rAAV-GFP transduction. These studies showed that cell morphology and S-100 immunoexpression (Fig. 3B), as well as p75 and GAP-43 immunostain (not shown), were not altered by rAAV-GFP transduction. Proliferation (BrdU incorporation) of Schwann cells of all three genotypes was slightly reduced by rAAV-GFP transduction (data not shown). These results allowed us to rule out the potential of an increase in cell proliferation resulting from rAAV-GFP transduction.

Tumorigenic Growth of $Nf1^{-/-}$ Schwann Cell Grafts

In our initial studies, embryonic Schwann cells (expressing GFP) of $Nf1^{-/-}$and $Nf1^{+/+}$ genotypes were syngrafted into the sciatic nerves of 10 adult wild-type mice (B6/$Nf1^{+/+}$). At time points ranging from 10 to 22 weeks postimplantation, no tumors were found in either $Nf1^{-/-}$or $Nf1^{+/+}$ Schwann cells grafts when *Nf1* wild-type mice were used as hosts. All of these grafts

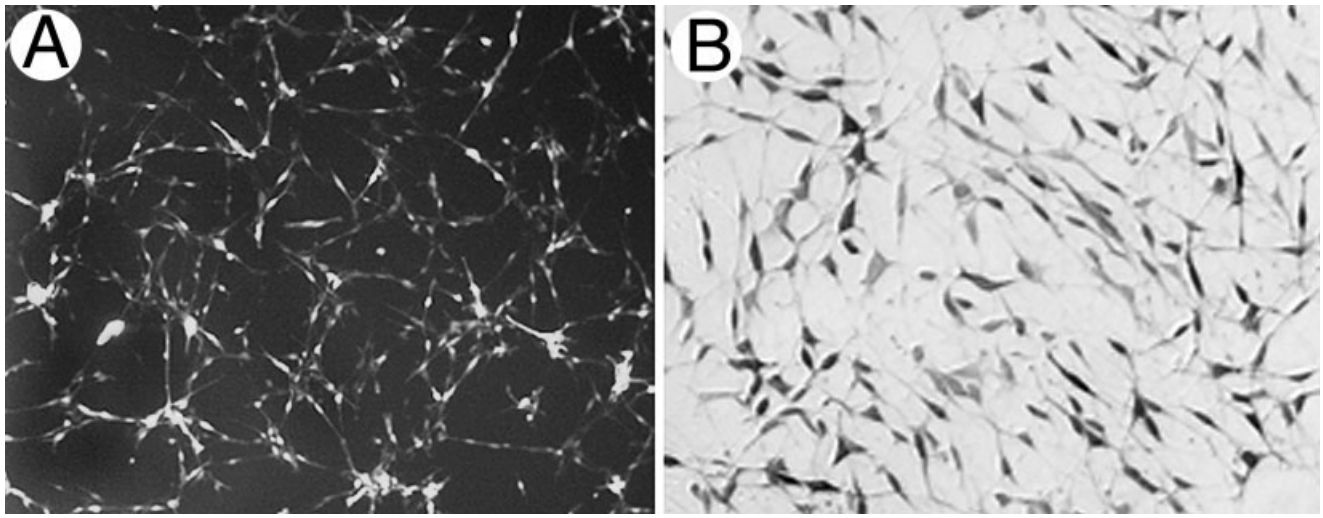

Fig. 3. AAV-mediated marker gene transduction into embryonic *Nf1* knockout Schwann cells. Mouse $Nf1^{+/+}$, $Nf1^{+/-}$, and $Nf1^{-/-}$ Schwann cells cultures were labeled with GFP by AAV-mediated gene transfection. **A:** Fluorescence microscopy of AAV-GFP transduced $Nf1^{-/-}$ Schwann cell cultures with MOI 1,000 at 9 days posttransduction. Greater than 95% cells in cultures showed green as examined under fluorescence microscopy with addition of a low level of regular light. **B:** S-100 immunostaining showed that rAAV transduced $Nf1^{-/-}$ cultures contained primarily Schwann cells that retained a normal spindle shape and phenotype. Identical results were obtained for cultures of all three genotypes. Original magnifications ×100 (A), ×200 (B).

exhibited limited GFP-positive cells and marginal hyperplastic lesions. Also, only sporadic mast cell accumulation was detected (data not shown). One explanation for this is that *Nf1* haploinsufficiency in host cells might be required to promote the growth of $Nf1^{-/-}$ Schwann cell grafts, but this was not tested directly. Alternatively, there was a possibility that transfection of embryonic Schwann cells with AAV-GFP might evoke an immune response affecting long-term growth. At this point, we had initiated the use of Schwann cells cultured from early crosses of B6/*Nf1* × 129/*Nf1* hybrid embryos as described above. Therefore, to eliminate concerns of immunorejection, all subsequent engrafting experiments were performed with immunodeficient *scid* mice with an $Nf1^{+/-}$ background (*scid*/$Nf1^{+/-}$) as hosts.

Twenty *scid*/$Nf1^{+/-}$ mice received bilateral nerve implants. $Nf1^{-/-}$ Schwann cells were implanted into one sciatic nerve, and $Nf1^{+/-}$ Schwann cells were implanted in the contralateral nerve. Engrafted nerves were examined for tumorigenic growth 2–12 weeks postimplantation. Within this time frame, nerve deformity and gross evidence of tumor growth were not observed. However, at the histological level, $Nf1^{-/-}$ Schwann cell grafts resulted in larger and more proliferative hyperplastic lesions compared with $Nf1^{+/-}$ grafts. Within 1 month postimplantation, marked hypercellularitity was associated with the $Nf1^{-/-}$ implants, but much less so with $Nf1^{+/-}$ Schwann cells (Fig. 4A,B). Also, after systemic injection of BrdU, more BrdU-positive cells were observed in all $Nf1^{-/-}$ Schwann cell implants than in the $Nf1^{+/-}$ Schwann cell implants (Fig. 4C,D). Double immunolabeling for BrdU and GFP confirmed that increased cell proliferation was strictly associated with the implanted $Nf1^{-/-}$ (GFP-positive) Schwann cells. Quantitative analysis of 1-month tumor grafts showed that $Nf1^{-/-}$ Schwann cells implants ($n = 8$) had 39 ± 16 BrdU-positive nuclei per high-power field and that $Nf1^{+/-}$ implants ($n = 8$) had 4 ± 1 (*t*-test, $P < 0.05$). This tenfold increase in proliferation indicates the heightened tumorigenic potential of $Nf1^{-/-}$ Schwann cells in vivo. Similar findings were obtained for transplants of $Nf1^{-/-}$ and $Nf1^{+/-}$ Schwann cells that were not transfected with AAV-GFP, confirming our previous in vitro observation that AAV-GFP transduction did not enhance tumorigenic growth.

Because neurofibromas develop slowly, we extended the planned survival time of a few surviving mice and examined the growth of *Nf1* knockout Schwann cells 6 months after engraftment to verify the tumorigenic growth of $Nf1^{+/-}$ Schwann cells. At this time point, tumor formation in nerves engrafted with $Nf1^{-/-}$ Schwann cells was immediately evident by gross enlargement near the injection site, whereas the contralateral nerves implanted with $Nf1^{+/-}$ Schwann cells (as control) appeared normal. In the three mice examined, the diameters of nerves engrafted with $Nf1^{-/-}$ Schwann cells were 1.5, 2.0, and 3.0 times greater than those of the same region of the control nerves. Histological examination revealed neurofibromas in nerves implanted with $Nf1^{-/-}$ Schwann cells (Fig. 5A), whereas only marginal hypercellularity was found in the control nerves (Fig. 5D). Also, GFP immunolabeling confirmed that the neurofibromas were associated with the $Nf1^{-/-}$ Schwann cells (Fig. 5B,E). Here the detection of GFP-labeled cells was unable to discern the extent of the hyperplastic lesion. This was likely attributable to the loss of GFP transgene after continued cell proliferation as described previously. Thus, GFP prelabeling

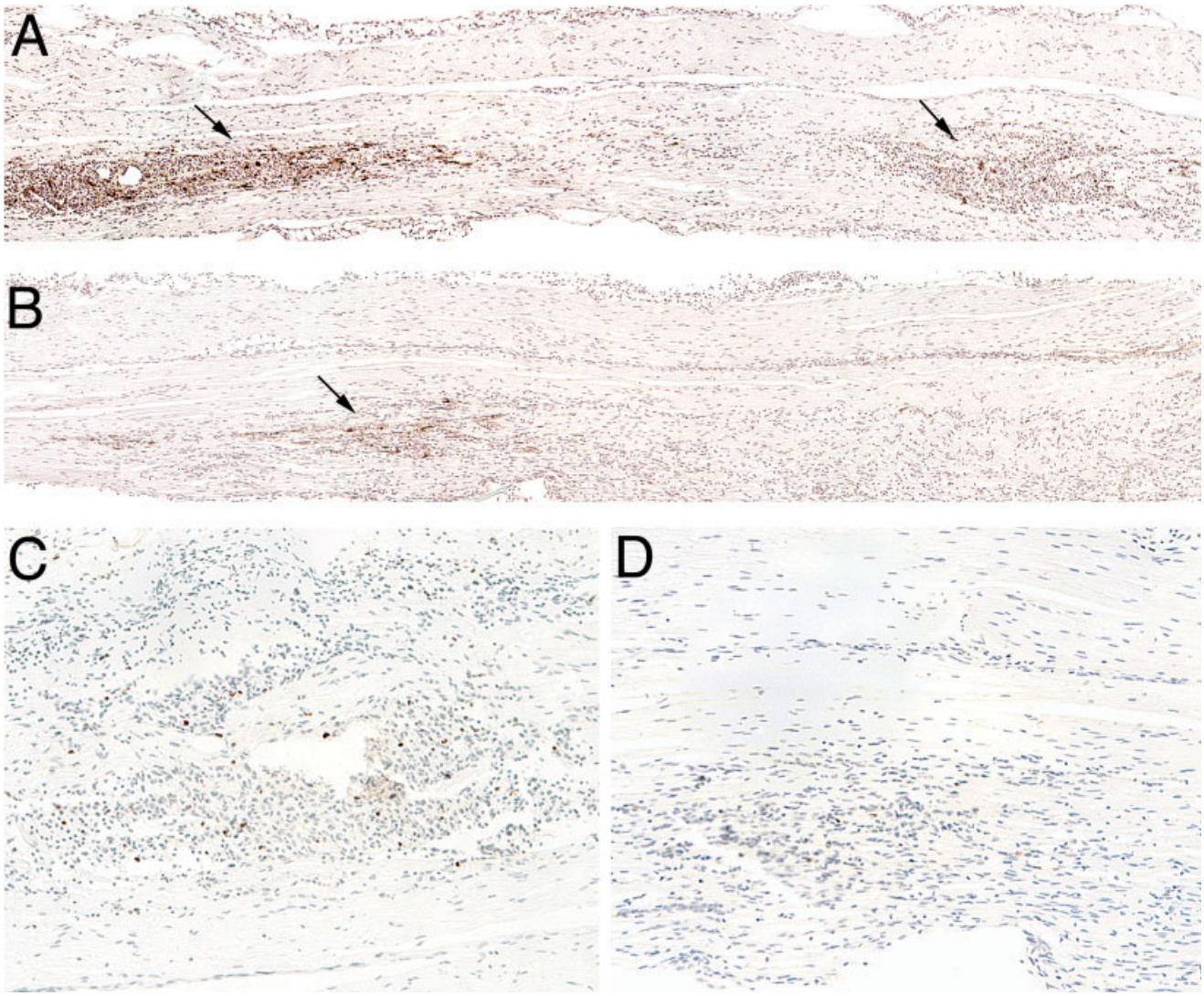

Fig. 4. Tumorigenic growth of $Nf1^{-/-}$ Schwann cells 2 weeks after implantation in the nerves of haploinsufficient mice. Embryonic $Nf1^{-/-}$ and $Nf1^{+/-}$ Schwann cells (5×10^5 cells) transduced with rAAV-GFP were bilaterally implanted into sciatic nerves of *scid*/$Nf1^{+/-}$ mice. Twenty-four hours before termination, mice received an IP injection of BrdU. At 2 weeks postimplantation, the engrafted nerves were immunostained for GFP (A,B) and BrdU (C,D), followed by a light hematoxylin counterstain. **A,C:** Implanted $Nf1^{-/-}$ Schwann cells appeared as multiple, intrafascicular, GFP-positive colonies (arrows), indicating migration and clonal expansion. Marked hypercellularity was associated with high BrdU incorporation. **B,D:** $Nf1^{+/-}$ Schwann cell implants showed only modest growth and proliferation. Original magnifications ×100 (A,B), ×200 (C,D).

may be used to track the development of implanted cell populations but might underestimate the full extent of cell proliferation and tumor progression. In addition, substantial numbers of BrdU-stained cells were present in the $Nf1^{-/-}$ Schwann cell masses (Fig. 5C), whereas this number was significantly lower for the $Nf1^{+/-}$ grafts (Fig. 5F). On average, the mitotic index of the 6-month $Nf1^{-/-}$ Schwann masses (58 ± 18) was nearly 12-fold greater than that of the $Nf1^{+/-}$ Schwann cell grafts (5 ± 1). Taken together, these findings indicate that $Nf1^{-/-}$ Schwann cells have a heightened tumorigenic potential in vivo and, given time, produce sizable neurofibromas.

More detailed immunohistochemical analysis of the tumor sections revealed that $Nf1^{-/-}$ Schwann cell tumors were observed as cellular infiltrates within the nerve fascicles, resulting in axon displacement (Fig. 6A). In addition to this intrafascicular growth, proliferative tumor masses were found extending beyond the perineurial margins (Fig. 6B). The tumor masses, both intraneural and extraneural, stained intensely for S-100, indicating that the masses consisted mostly of Schwann cells (Fig. 6C). There was also an increase in mast cells associated with these tumors (Fig. 6D). Both infiltrative and expansive tumor masses showed evidence of high vascularity and angiogenesis

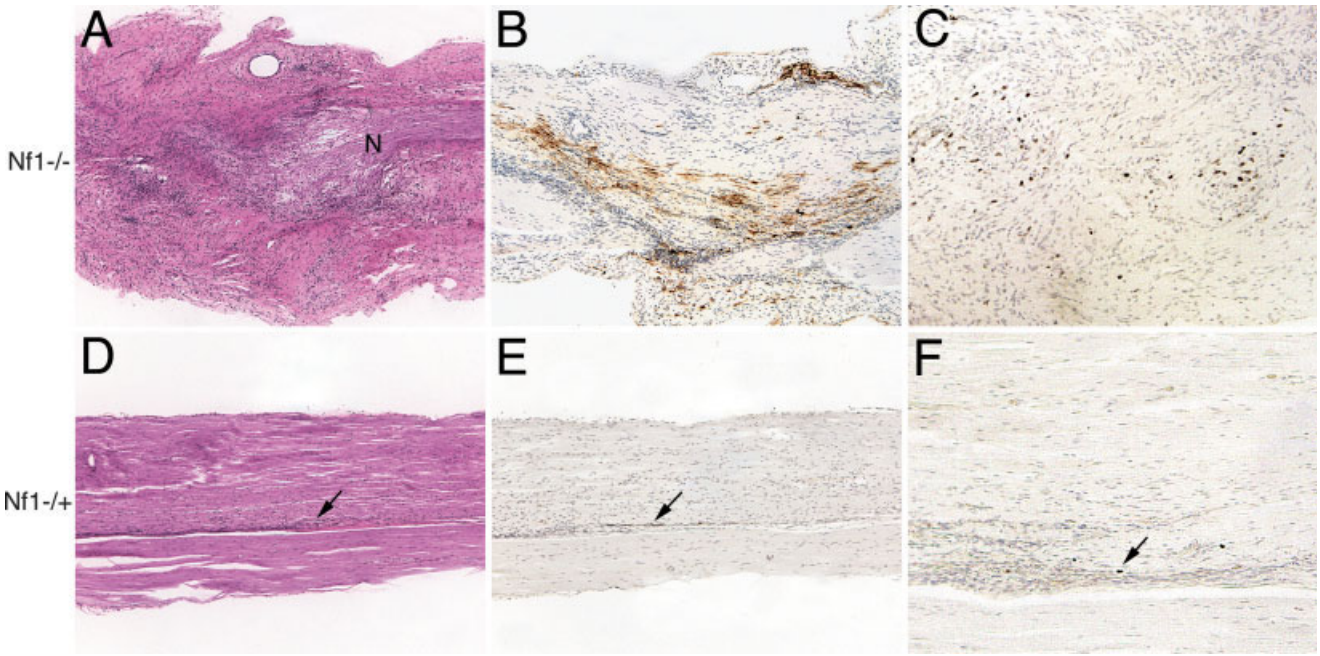

Fig. 5. Tumorigenic growth by $Nf1^{-/-}$ Schwann cells. Embryonic *Nf1* knockout Schwann cells were implanted into sciatic nerves of *scid*/$Nf1^{+/-}$ mice as described for Figure 4. At 6 months posttransplantation, sections of the engrafted nerves were stained with hematoxylin and eosin (A,D) and immunostained for GFP (B,E) and BrdU (C,F). **A–C:** $Nf1^{-/-}$ Schwann cell implants formed tumors resembling plexiform neurofibroma. The nerve (N) was severely disrupted and consumed by tumor. B: GFP-positive cells, despite waning transduction, circumscribed the expanding neoplasia. C: BrdU incorporation remained high, especially in the tumor margins. **D–F:** $Nf1^{+/-}$ Schwann cells implants showed no significant long-term tumorigenic growth, although small colonies persisted, and occasional mitosis were found (arrows). Original magnifications ×100 (A,B,D,E), ×200 (C,F).

(Fig. 6E,F). Overall, the features of the $Nf1^{-/-}$ tumors resembled those of plexiform neurofibroma.

DISCUSSION

It was previously reported that $Nf1^{-/-}$ Schwann cells isolated from *Nf1* mutant embryos prior to death (E12.5) have enhanced invasive and angiogenic properties but a disadvantage of growth compared with wild-type Schwann cells (Kim et al., 1995; 1997). Although the transformed $Nf1^{-/-}$ Schwann cells ($Nf1^{-/-}$ TXF) exhibited hyperplasia in vitro when exposed to forskolin or withdrawal of serum from the culture medium (Kim et al., 1997), they did not show tumor formation in mouse nerve (Rizvi et al., 2002), in contrast to our results. We found $Nf1^{-/-}$ Schwann cells (both SSC and FSC) showed a growth advantage in medium not only with low levels of serum but also with high levels of serum and no forskolin. Thus the different observations between reported results (Kim et al., 1995, 1997) and our results is unlikely due to the culture medium used but, most likely, at least in part, is due to the variations between mice strain and litters. We found that culture of mouse embryonic Schwann cells is often associated with significant variation in cell proliferation between cultures from different litters. Thus the growth advantage of $Nf1^{-/-}$ Schwann cells can be easily offset if the proliferation rate of $Nf1^{-/-}$ Schwann cells from one litter is compared with that of $Nf1^{+/-}$ or wild-type Schwann cells from a different litter. Such variations had been problematic in the study of *Nf1* astrocyte cultures, and a solution was obtained when pooled $Nf1^{+/-}$ and $Nf1^{+/+}$ matched littermate astrocyte cultures were used (Gutmann et al., 1999; Bajenaru et al., 2001). Hence the growth advantage of $Nf1^{-/-}$ Schwann cells is due to the cellular alterations resulting from the *Nf1* mutation, a cell-autonomous growth advantage. As with other $Nf1^{-/-}$ cells, including mast cells (Ingram et al., 2000, 2001), astrocytes (Bajenaru et al., 2001), and hematopoietic cells (Zhang et al., 2001), loss of *Nf1* function in Schwann cells promotes proliferation via up-regulation of certain growth factors stimulated through the increased ras or other activity (Mashour et al., 1999; Kim et al., 2001). Although the increased proliferation of $Nf1^{-/-}$ Schwann cells does not lead to immortalization in vitro, the cells are less dependent on ectopic sources of growth factor(s) and may lead to tumorigenic growth in vivo. Also, the fact that the $Nf1^{-/-}$ Schwann cell cultures senesce at very low passage numbers might indicate that their in vivo tumorigenic behavior is dependent on paracrine influence. Similarly, $NF1^{-/-}$ Schwann cell cultures (derived from human neurofibromas) infrequently establish as stable cell lines but can show tumorigenic growth as xenografts (Muir et al., 2001). It should be noted that rapid culture senescence is not a behavior exclusive to Schwann cells or neurofibromin-deficient cells. This phenomenon is frequently observed in the culture of tissues from certain species (particularly mouse) and many tumors (even malignancies).

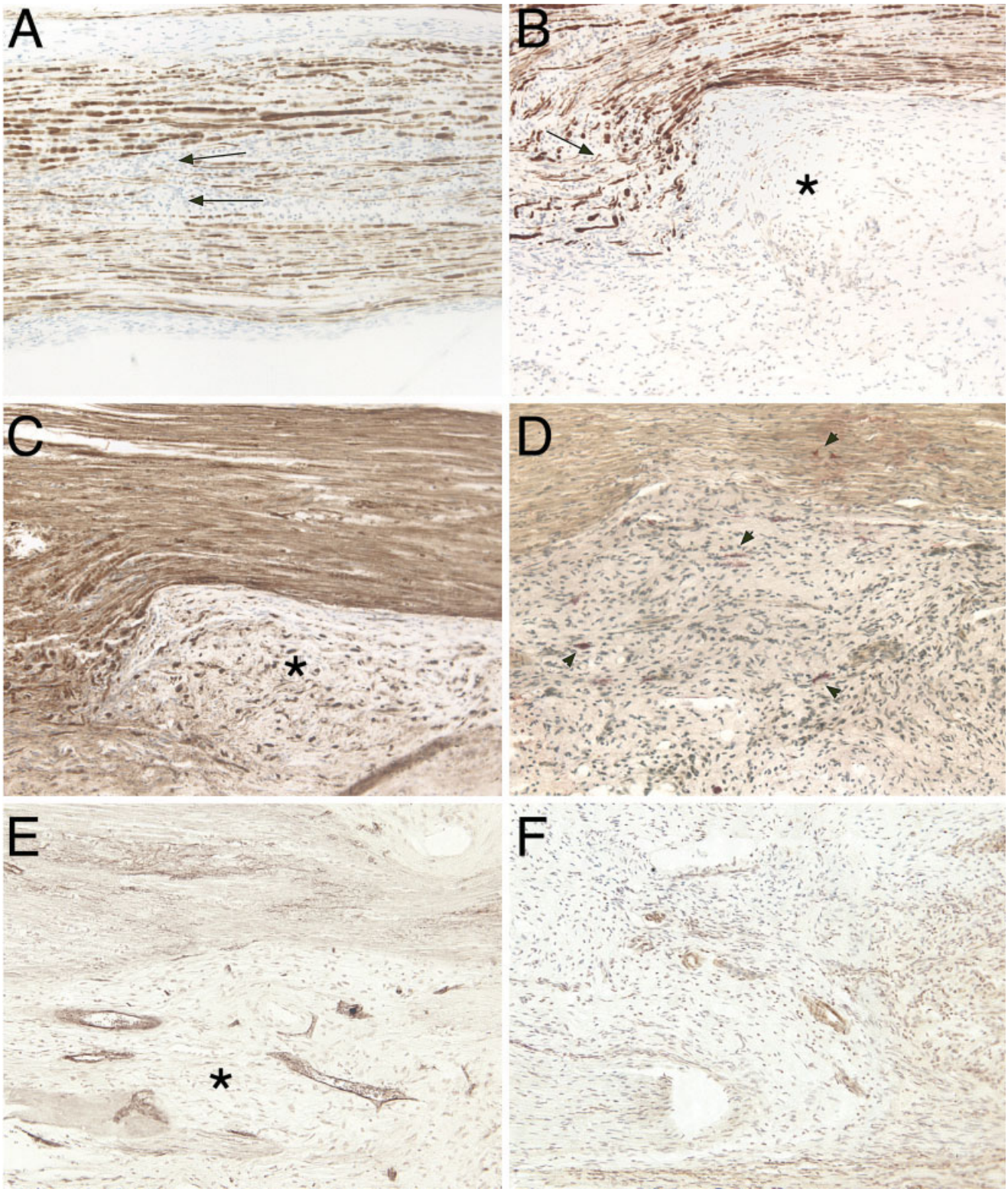

Fig. 6. Neurofibroma formation by $Nf1^{-/-}$ Schwann cells 6 months after implantation into *sad/Nf1* $^{+/-}$ mouse nerves. Sections of the engrafted nerves were immunostained for neurofilaments (A,B), S-100 (C), and endothelial cell antigens vWF and FLK (E,F). **A:** $Nf1^{-/-}$ Schwann cell tumors were observed as cellular infiltrates within the nerve fascicles, resulting in axon displacement (arrows). **B:** In addition to intrafascicular growth, proliferative tumor masses were found extending beyond the perineurial margins (asterisks). **C:** Tumor masses contained Schwann cells embedded in extracellular matrix. **D:** Mast cell infiltration (arrowheads) was associated with neurofibroma formation (Leder stain, hematoxylin). **E,F:** Tumor masses and infiltrative colonies were highly vascularized. Original magnification ×200.

Recently developed genetic mouse models that develop plexiform neurofibromas when the *Nf1* gene is knocked out in all Schwann cells (Zhu et al., 2002) or in a group of mixed cell types (Cichowski et al., 1999) have yielded important insights into neurofibroma formation. However, genetically engineered mouse cancer models that create fields of mutant cells do not recapitulate the human circumstances in which clonal outgrowth occurs from a single mutant precursor. For example, plexiform neurofibromas derive only from sensory ganglia and cranial nerves in mouse, unlike the human situation. These models also take up to 1 year for tumors to develop, and the tumor sites are unpredictable. Our examination of $Nf1^{-/-}$ Schwann cells engrafted into $Nf1^{+/-}$ nerves up to 12 weeks postimplantation showed limited growth and no significant tumor masses, which is similar to the observations by Rizvi et al. (2002). However, more detailed histological and immunohistochemical analysis showed that $Nf1^{-/-}$ Schwann cells syngrafts have significantly increased cellularity and mitotic index compared with control grafts, indicating a potential tumorigenic growth. Such tumorigenic potential was further confirmed by the long-term grafts (at 6 months) where tumorigenic growth was unmistakable. The increased mitotic index from $Nf1^{-/-}$ Schwann cell syngrafts appeared to be comparable between long-term and short-term implantation, confirming a persistent tumorigenic growth. Moreover, the histopathology of these syngraft tumors, as with that found in recent genetic (Cichowski et at., 1999; Vogel et al., 1999; Zhu et al., 2002) and xenograft (Muir et al., 2001) mouse models exhibits many characteristics of human plexiform neurofibromas (Kleihues and Cavenee, 2000). In contrast, syngrafted $Nf1^{+/-}$ Schwann cells are not expansive and actually decrease over time, indicating that they are not tumorigenic. Although injury-induced tumor growth has been found occasionally in $Nf1^{+/-}$ mice following nerve transection (Rizvi et al., 2002), the absence of tumor formation in our $Nf1^{+/-}$ Schwann cell grafts makes it very unlikely that the cell injection per se or any allogenic response initiated tumorigenic growth by the engrafted $Nf1^{-/-}$ Schwann cells.

Human neurofibroma Schwann cells, in contrast to Schwann cells from normal nerve, can invade extracellular matrices and grow without associating with axons (Kamata 1978; Muir, 1995; Kim et al., 1997). Similarly, syngrafted $Nf1^{-/-}$ Schwann cells proliferated and grew without axonal contact. The increased mast cell infiltration is a well-known pathological characteristic of human neurofibromas. Accordingly, abundant mast cell infiltration was also found in the $Nf1^{+/-}$ host but not in wild-type host after $Nf1^{-/-}$ Schwann cell implantation. With $Nf1^{+/-}$ mouse hosts receiving bilateral implants, we found no distinct difference in mast cell infiltration between nerves engrafted with $Nf1^{-/-}$ vs. $Nf1^{+/-}$ Schwann cells. However, with this grafting model, we cannot rule out the possibility that the mast cell infiltration observed in response to the engrafted cells resulted from an allogeneic response that indirectly drives the tumorigenicity of the $Nf1^{-/-}$ cells. On the other hand, such an allogenic response is not likely to be a primary effect, and *Nf1* haploinsufficient mast cells are known attraction to factors secreted by $Nf1^{-/-}$ Schwann cells (Ingram et al., 2000, 2001; Zhu et al., 2002; Yang et al., 2003). In addition, human neurofibromas express abundant angiogenic factors and show high vascularity (Arbiser et al., 1998; Kawachi et al., 2003). Similarly, $Nf1^{-/-}$ tumors formed in $Nf1^{+/-}$ mice were also highly vascularized, suggesting that interactions between $Nf1^{-/-}$ Schwann cells and $Nf1^{+/-}$ endothelial cells might also play an important role in tumorigenesis. It remains to be determined whether such tumorigenic behavior is dependent on specific paracrines or whether $Nf1^{+/-}$ endothelial cells are particularly responsive to the angiogenic signals produced by $Nf1^{-/-}$ Schwann cells. Overall, for each aspect examined, we found that these syngraft neurofibromas recapitulate the growth of human plexiform neurofibromas.

Our work is the first to achieve tumorigenic growth in vivo by intraneural implantation of mouse embryonic $Nf1^{-/-}$ Schwann cells. There is no noticeable functional impairment, mortality, or symptoms of graft-vs.-host disease (e.g., hair loss, diarrhea) associated with the implantation for 6 months, providing a reliable and sustained growth of $Nf1^{-/-}$ Schwann cell in syngraft nerves.

This model more precisely recapitulates the initiating lesion in *NF1* patients, and tumor occurs at a known location. Therefore, this system can be used to characterize early events in tumorigenesis and to test new therapies. In addition, this syngraft model suggests that embryonic development is not essential for tumorigenic growth of embryonic $Nf1^{-/-}$ Schwann cells. Furthermore, toward potential application of gene therapy, we also have shown a high efficiency of GFP transduction into Schwann cells with AAV vector-mediated gene transfer. This approach may facilitate the development of antiangiogenic gene therapy to negate the sustained growth of neurofibroma.

ACKNOWLEDGMENTS

We thank Dr. Anthony Yachnis for sharing his expertise in histopathology. Xuelian Zhang, Debbie Neubauer, Elizabeth Baldwin, Marisa Scott, and James Graham provided technical assistance. This study was supported by grants DAMD 170010549 (to D.M.) and DAMD 170110707 (to M.R.W.) funded by the U.S. Army Neurofibromatosis Research Program.

REFERENCES

Arbiser JL, Flynn E, Barnhill RL. 1998. Analysis of vascularity of human neurofibromas. J Am Acad Dermatol 38:950–954.

Bajenaru ML, Donahoe J, Corral T, Reilly KM, Brophy S, Pellicer A, Gutmann DH. 2001. Neurofibromatosis 1 (NF1) heterozygosity results in a cell-autonomous growth advantage for astrocytes. Glia 33:314–323.

Ballester R, Marchuk D, Boguski M, Saulino A, Letcher R, Wigler M, Collins F. 1990. The NF1 locus encodes a protein functionally related to mammalian GAP and yeast IRA proteins. Cell 63:851–859.

Blunt T, Gell D, Fox M, Taccioli GE, Lehmann AR, Jackson SP, Jeggo PA. 1996. Identification of a nonsense mutation in the carboxyl-terminal region of DNA-dependent protein kinase catalytic subunit in the scid mouse. Proc Natl Acad Sci U S A 93:10285–10290.

Brannan CI, Perkins AS, Vogel KS, Ratner N, Nordlund ML, Reid SW, Buchberg AM, Jenkins NA, Parada LF, Copeland NG. 1994. Targeted disruption of the neurofibromatosis type-1 gene leads to developmental abnormalities in heart and various neural crest-derived tissues. Genes Dev 8:1019–1029.

Cichowski K, Shih TS, Schmitt E, Santiago S, Reilly K, McLaughlin ME, Bronson RT, Jacks T. 1999. Mouse models of tumor development in neurofibromatosis type 1. Science 286:2172–2176.

Colman SD, Williams CA, Wallace MR. 1995. Benign neurofibromas in type 1 neurofibromatosis (NF1) show somatic deletions of the NF1 gene. Nat Genet 11:90–92.

Dong Z, Sinanan A, Parkinson D, Parmantier E, Mirsky R, Jessen KR. 1999. Schwann cell development in embryonic mouse nerves. J Neurosci Res 56:334–348.

Erlandson RA, Woodruff JM. 1982. Peripheral nerve sheath tumors: an electron microscopic study of 43 cases. Cancer 49:273–287.

Ferguson TA, Muir D. 2000. MMP-2 and MMP-9 increase the neurite-promoting potential of schwann cell basal laminae and are upregulated in degenerated nerve. Mol Cell Neurosci 16:157–167.

Gutmann DH, Loehr A, Zhang Y, Kim J, Henkemeyer M, Cashen A. 1999. Haploinsufficiency for the neurofibromatosis 1 (NF1) tumor suppressor results in increased astrocyte proliferation. Oncogene 18:4450–4459.

Ingram DA, Yang FC, Travers JB, Wenning MJ, Hiatt K, New S, Hood A, Shannon K, Williams DA, Clapp DW. 2000. Genetic and biochemical evidence that haploinsufficiency of the Nf1 tumor suppressor gene modulates melanocyte and mast cell fates in vivo. J Exp Med 191:181–188.

Ingram DA, Hiatt K, King AJ, Fisher L, Shivakumar R, Derstine C, Wenning MJ, Diaz B, Travers JB, Hood A, Marshall M, Williams DA, Clapp DW. 2001. Hyperactivation of p21(ras) and the hematopoietic-specific Rho GTPase, Rac2, cooperate to alter the proliferation of neurofibromin-deficient mast cells in vivo and in vitro. J Exp Med 194:57–69.

Jacks T, Shih TS, Schmitt EM, Bronson RT, Bernards A, Weinberg RA. 1994. Tumour predisposition in mice heterozygous for a targeted mutation in Nf1. Nat Genet 7:353–361.

Kamata Y. 1978. Study on the ultrastructure and acetylcholinesterase activity in von Recklinghausen's neurofibromatosis. Acta Pathol Jpn 28:393–410.

Kawachi Y, Xu X, Ichikawa E, Imakado S, Otsuka F. 2003. Expression of angiogenic factors in neurofibromas. Exp Dermatol 12:412–417.

Kim HA, Rosenbaum T, Marchionni MA, Ratner N, DeClue JE. 1995. Schwann cells from neurofibromin deficient mice exhibit activation of p21ras, inhibition of cell proliferation and morphological changes. Oncogene 11:325–335.

Kim HA, Ling B, Ratner N. 1997. *Nf1*-deficient mouse Schwann cells are angiogenic and invasive and can be induced to hyperproliferate: reversion of some phenotypes by an inhibitor of farnesyl protein transferase. Mol Cell Biol 17:862–872.

Kim HA, Ratner N, Roberts TM, Stiles CD. 2001. Schwann cell proliferative responses to cAMP and *Nf1* are mediated by cyclin D1. J Neurosci 21:1110–1116.

Kleihues P, Cavenee WK. 2000. Pathology and genetics of tumors of the nervous system. Lyon, France: IARC Press.

Knudson AG. 2000. Chasing the cancer demon. Annu Rev Genet 34:1–19.

Korf BR. 1999. Plexiform neurofibromas. Am J Med Genet 89:31–37.

Mashour GA, Wang HL, Cabal-Manzano R, Wellstein A, Martuza RL, Kurtz A. 1999. Aberrant cutaneous expression of the angiogenic factor midkine is associated with neurofibromatosis type-1. J Invest Dermatol 113:398–402.

Muir D. 1994. Metalloproteinase-dependent neurite outgrowth within a synthetic extracellular matrix is induced by nerve growth factor. Exp Cell Res 210:243–252.

Muir D. 1995. Differences in proliferation and invasion by normal, transformed and NF1 Schwann cell cultures are influenced by matrix metalloproteinase expression. Clin Exp Metast 13:303–314.

Muir D, Varon S, Manthorpe M. 1990. Schwann cell proliferation in vitro is under negative autocrine control. J Cell Biol 111:2663–2671.

Muir D, Johnson J, Rojiani M, Inglis BA, Rojiani A, Maria BL. 1996. Assessment of laminin-mediated glioma invasion in vitro and by glioma tumors engrafted within rat spinal cord. J Neurooncol 30:199–211.

Muir D, Neubauer D, Lim IT, Yachnis AT, Wallace MR. 2001. Tumorigenic properties of neurofibromin-deficient neurofibroma Schwann cells. Am J Pathol 158:501–513.

Peltonen J, Jaakkola S, Lebwohl M, Renvall S, Risteli L, Virtanen I, Uitto J. 1988. Cellular differentiation and expression of matrix genes in type 1 neurofibromatosis. Lab Invest 59:760–771.

Rasmussen SA, Overman J, Thomson SA, Colman SD, Abernathy CR, Trimpert RE, Moose R, Virdi G, Roux K, Bauer M, Rojiani AM, Maria BL, Muir D, Wallace MR. 2000. Chromosome 17 loss-of-heterozygosity studies in benign and malignant tumors in neurofibromatosis type 1. Genes Chromosomes Cancer 28:425–431.

Riccardi VM. 1992. Neurofibromatosis: phenotype, natural history, and pathogenesis. Baltimore: Johns Hopkins University Press.

Rizvi TA, Huang Y, Sidani A, Atit R, Largaespada DA, Boissy RE, Ratner N. 2002. A novel cytokine pathway suppresses glial cell melanogenesis after injury to adult nerve. J Neurosci 22:9831–9840.

Rutkowski JL, Wu K, Gutmann DH, Boyer PJ, Legius E. 2000. Genetic and cellular defects contributing to benign tumor formation in neurofibromatosis type 1. Hum Mol Genet 9:1059–1066.

Serra E, Rosenbaum T, Winner U, Aledo R, Ars E, Estivill X, Lenard HG, Lazaro C. 2000. Schwann cells harbor the somatic NF1 mutation in neurofibromas: evidence of two different Schwann cell subpopulations. Hum Mol Genet 9:3055–3064.

Upadhyaya M, Han S, Consoli C, Majounie E, Horan M, Thomas NS, Potts C, Griffiths S, Ruggieri M, von Deimling A, Cooper DN. 2004. Characterization of the somatic mutational spectrum of the neurofibromatosis type 1 (NF1) gene in neurofibromatosis patients with benign and malignant tumors. Hum Mutat 23:134–146.

Vogel KS, Klesse LJ, Velasco-Miguel S, Meyers K, Rushing EJ, Parada LF. 1999. Mouse tumor model for neurofibromatosis type 1. Science 286:2176–2179.

Xu GF, O'Connell P, Viskochil D, Cawthon R, Robertson M, Culver M, Dunn D, Stevens J, Gesteland R, White R, Weiss R. 1990. The neurofibromatosis type 1 gene encodes a protein related to GAP. Cell 62:599–608.

Yang FC, Ingram DA, Chen S, Hingtgen CM, Ratner N, Monk KR, Clegg T, White H, Mead L, Wenning MJ, Williams DA, Kapur R, Atkinson SJ, Clapp DW. 2003. Neurofibromin-deficient Schwann cells secrete a potent migratory stimulus for $Nf1^{+/-}$ mast cells. J Clin Invest 112:1851–1861.

Zhang Y, Taylor BR, Shannon K, Clapp DW. 2001. Quantitative effects of Nf1 inactivation on in vivo hematopoiesis. J Clin Invest 108:709–715.

Zhu Y, Ghosh P, Charnay P, Burns DK, Parada LF. 2002. Neurofibromas in NF1: Schwann cell origin and role of tumor environment. Science 296:920–922.

Oncogene (2006) 25, 2297–2303

www.nature.com/onc

ORIGINAL ARTICLE

Nf1 haploinsufficiency augments angiogenesis

M Wu[1], MR Wallace[2,3] and D Muir[1,3]

[1]*Department of Pediatrics, Division of Neurology, University of Florida, Gainesville, FL, USA;* [2]*Department of Molecular Genetics and Microbiology, University of Florida, Gainesville, FL, USA and* [3]*McKnight Brain Institute and UF Shands Cancer Center, University of Florida, Gainesville, FL, USA*

Mutations in the *NF1* tumor-suppressor gene underlie neurofibromatosis type 1 (NF1), in which patients are predisposed to certain tumors such as neurofibromas and may associate with vascular disorder. Plexiform neurofibromas are slow growing benign tumors that are highly vascular and can progress to malignancy. The development of neurofibromas requires loss of both *Nf1* alleles in Schwann cells destined to become neoplastic and may be exacerbated by *Nf1* heterozygosity in other non-neoplastic cells. This study tested the hypothesis that *Nf1* heterozygosity exaggerates angiogenesis. We found that *Nf1* heterozygous mice showed increased neovascularization in both the retina and cornea in response to hypoxia and bFGF, respectively, compared to their wild-type littermates. The increase in corneal neovascularization was associated with heightened endothelial cell proliferation and migration, and increased infiltration of inflammatory cells. In addition, *Nf1* heterozygous endothelial cell cultures showed an exaggerated proliferative response to angiogenic factors, particularly to bFGF. These findings support the conclusion that *Nf1* heterozygosity in endothelial cells and perhaps inflammatory cells augments angiogenesis, which may promote neurofibroma formation in NF1.
Oncogene (2006) **25,** 2297–2303. doi:10.1038/sj.onc.1209264; published online 14 November 2005

Keywords: neurofibromatosis; vasculature; Nf1 haploinsufficiency; endothelial cell; inflammatory cells

Introduction

Mutations in the *NF1* gene cause neurofibromatosis type 1 (NF1), a common dominantly inherited disease that occurs in one out of 3500 individuals worldwide. The *NF1* gene encodes the tumor-suppressor protein neurofibromin that harbors a functional Ras-guanosine triphosphatase-activating protein (GAP) domain (Ballester *et al*., 1990; Xu *et al*., 1990). Individuals with NF1 are predisposed to certain tumors, including benign neurofibromas, malignant peripheral nerve sheath tumor (MPNST), pheochromocytoma, astrocytoma, and juvenile myelomonocytic leukemia (Side and Shannon, 1998), that occur in the context of *Nf1* heterozygous ($Nf1^{+/-}$) tissues. The hallmark feature is neurofibromas, and plexiform neurofibromas and MPNST (often arising from plexiform tumors) can be life threatening. To date, there are no reliable medical treatments to prevent or attenuate their growth. In the peripheral and central nervous system, biallelic *Nf1* inactivation in Schwann cells or astrocytes can initiate tumor formation in the presence of $Nf1^{+/-}$ cells, suggesting an important role of $Nf1^{+/-}$ stromal cells in promoting tumor formation (Zhu *et al*., 2002; Bajenaru *et al*., 2003; Wu *et al*., 2005).

Because solid tumor foci cannot expand without angiogenesis to create new blood vessel supply, antiangiogenic therapies have been pursued as potential strategies for cancer treatment. Targeting endothelial cells rather than actual tumor cells is widely applicable to various tumors, especially slow growing neoplasms like neurofibromas that do not respond to conventional cancer treatments. Also, antiangiogenic therapy may be particularly relevant to neurofibromas because they are highly vascularized (Arbiser *et al*., 1998; Morello *et al*., 2001; Wolkenstein *et al*., 2001). Neurofibromin-deficient Schwann cells have increased Ras activity and a heightened angiogenic potential which most likely promotes vascularization and growth of NF1 tumors (Sheela *et al*., 1990). Angiogenic properties have been described for *Nf1* null Schwann cells derived from NF1 tumors and *Nf1* knockout mice (Sheela *et al*., 1990; Kim *et al*., 1997; Mashour *et al*., 1999, 2001), and from their xenografts and syngrafts in mice models (Duprez *et al*., 1991; Wu *et al*., 2005). Although *NF1* heterozygosity has been implicated in the growth of NF1 tumors, its contribution to vascularization and associated cellular responses remains speculative.

We report here that *Nf1* heterozygous endothelial cell cultures have an exaggerated proliferative response to several angiogenic factors. Moreover, *Nf1* heterozygous mice show greater angiogenesis in response to various angiogenic stimuli in both the retinal neovascularization (NV) and corneal NV models. We also found that increased corneal NV was associated with heightened endothelial cell proliferation and migration, and elevated infiltration of inflammatory cells including macrophages and mast cells.

Correspondence: Dr M Wu, Department of Pediatrics/Neuro, University of Florida College of Medicine, Box 100296, Gainesville, FL 32610 USA.
E-mail: wumin@ufl.edu
Received 2 August 2005; revised 13 October 2005; accepted 13 October 2005; published online 14 November 2005

Results

Nf1$^{+/-}$ mice exhibit an exaggerated ischemia-induced retinal neovascular response

To determine whether *Nf1* heterozygosity affects angiogenic responses, we used a mouse retinal NV model, which has been routinely used for retinopathy studies (Raisler *et al*., 2002). In response to hypoxia condition, retinas from heterozygous mice had more neovascular endothelial cells associated with aberrant microvessels penetrating the internal limiting membrane (Figure 1a) than wild-type mice. Quantitative scoring indicated that *Nf1*$^{+/-}$ retinas ($n=25$) had significantly increased (52%) neovascularity compared to *Nf1*$^{+/+}$ retinas ($n=6$, $P=0.008$) (Figure 1b). However, in the control condition (normoxia), the age-matched mice showed no significant difference in their baseline retinal NV between the two genotypes examined ($n=8$ each) (data not shown), indicating that *Nf1*$^{+/-}$ mice are free of intrinsic aberrant retinal NV. With baseline correction (subtracting the score of control mice from those of treated mice), *Nf1*$^{+/-}$ mice showed a 66% increase in retinal NV compared to wild-type mice. These data indicate that *Nf1* heterozygosity may, in general, exaggerate the angiogenic response.

Nf1$^{+/-}$ mice exhibit an exaggerated corneal neovascular response

Next, we examined the angiogenic response of *Nf1*$^{+/-}$ mice in the mouse corneal NV model. We first examined the specificity of the corneal NV response to micropellets implanted with bFGF. Pellets containing 0, 31 and 90 ng of bFGF were implanted into the corneas of *Nf1*$^{+/-}$ mice. After 6 days, corneas implanted with pure pellet showed no vessel formation (not shown). Corneas implanted with bFGF-impregnated pellets induced abundant new blood vessel growth extending from limbal vessels and advancing toward the implantation site (Figure 2a). Confocal fluorescence microscopy of CD31 immunostained corneas showed markedly greater NV (both maximum new vessel length and outgrowth circumference) in response to 96 ng bFGF (Figure 2b) compared to 31 ng pellets (Figure 2c). These data confirmed that the corneal NV induced in *Nf1*$^{+/-}$ mice is bFGF specific and dose dependent, and thus may provide a sensitive and reliable means to assess the effect of *Nf1* haploinsufficiency on angiogenesis. The higher dose pellets were used in all subsequent testing.

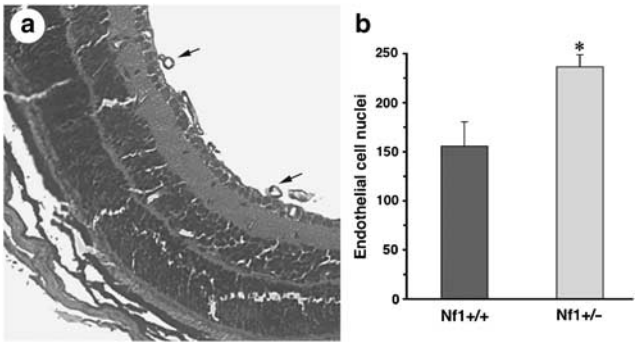

Figure 1 Retinal NV response to experimental hypoxia. Litters of *Nf1*$^{+/-}$ and *Nf1*$^{+/+}$ mice were exposed to a high oxygen atmosphere for 5 days followed by 5 days in a normal atmosphere. (**a**) NV was assessed in H&E-stained sections of whole eyes from *Nf1*$^{+/-}$ and *Nf1*$^{+/+}$ mice by counting endothelial cell nuclei associated with new blood vessels that penetrated the interlimiting membrane into the vitreous space (arrows). (**b**) Scores of the retinal NV were obtained by adding the total number of neovascular endothelial cell nuclei found in eight sections of each eye. Data represent the means (+s.e.) of six wild-type and 25 *Nf1*$^{+/-}$ retinas from triplicate experiments. *$P=0.008$, ANOVA. Original magnification: $\times 200$.

Corneal NV induced by bFGF was compared between *Nf1*$^{+/-}$ and *Nf1*$^{+/+}$ mice. At 6 days after implantation the corneal NV in *Nf1* heterozygous mice was conspicuously greater than that found in wild-type littermates (Figure 2b and d). The maximum new blood vessel length in corneas of *Nf1* heterozygous mice was 67% greater than that of wild-type controls ($P=0.00002$, $n=13$) (Figure 2e). There was no significant difference in the circumferences of NV (Figure 2f) or in the NV response 4 days after bFGF implantation (data not shown) between *Nf1* heterozygous and wild-type littermates. These findings indicate that the effect of *Nf1* heterozygosity on angiogenesis is cumulative and complex (not a simple dose response). Taken together, the results obtained using two *in vivo* assays provide convincing evidence that *Nf1* haploinsufficiency significantly increased the angiogenic response to hypoxia or bFGF, without nonspecific baseline effects.

Corneal NV is associated with greater endothelial cell proliferation in Nf1$^{+/-}$ mice

We tested the hypothesis that heightened endothelial cell proliferation is associated with the corneal NV response in *Nf1* haploinsufficient mice. At 6 days after bFGF implantation, endothelial cell proliferation was assessed in cross-sections of corneas from *Nf1* heterozygous and wild-type littermates by double labeling for Ki67 and CD31. In the entire region from the limbus to the pellet site, more than twice the number of proliferating endothelial (double labeled) cells was observed in the corneas of *Nf1* heterozygous mice compared to wild-type mice ($P=0.001$, $n=8$) (Figure 3a). The greatest difference was found in more distal zones from the limbus, where the number of proliferating CD31-positive cells was more than fivefold greater in *Nf1*$^{+/-}$ corneas than in wild-type controls. These results indicate that endothelial cell proliferation and migration in response to bFGF is exaggerated by *Nf1* haploinsufficiency.

We then examined the response of *Nf1*$^{+/-}$ endothelial cells to mitogens *in vitro*. Endothelial cell cultures were established from microvessels isolated from *Nf1*$^{+/-}$ and wild-type littermates. Endothelial cell phenotype was confirmed by immunoexpression of Von Willebrand's Factor and abundant tube formation in Matrigel three-dimensional culture (results not shown). In a base medium (containing serum but no endothelial cell mitogen supplements) approximately 5% of the wild-type endothelial cells had BrdU-positive nuclei

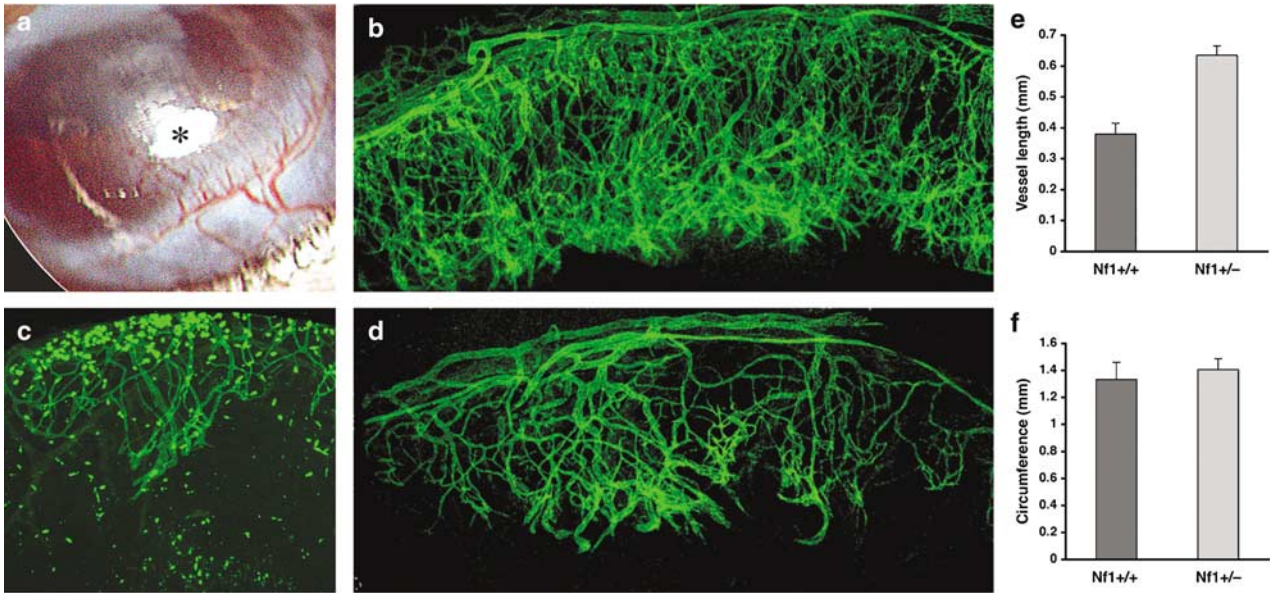

Figure 2 *Nf1*$^{+/-}$ mice exhibit increased growth factor-induced corneal neovascularization. Micropellets impregnated with bFGF were implanted into the corneal stroma of *Nf1*$^{+/-}$ (**a**–**c**) and *Nf1*$^{+/+}$ (**d**) mice. At 6 days postimplantation an intense neovascular response was seen originating from the limbal vessels and extending to the pellet (*) (**a**). Neovascularization was observed by fluorescence confocal microscopy of CD31-immunostained corneal flat-mounts 6 days after implantation of micropellets containing 96 ng (**b** and **d**) and 31 ng (**c**) bFGF. Corneal NV was quantified by measuring the maximum vessel length (**e**) extending from the base of the limbal vascular plexus toward the pellet and the maximum contiguous circumference (**f**) along the base of the limbal of neovascularization zone. Data represent the means (+s.e.; $n=13$) obtained from three independent experiments. Original magnification: ×100 (**b**–**d**).

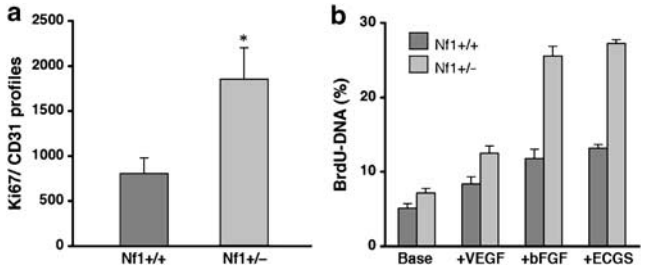

Figure 3 Increased proliferation of *Nf1*$^{+/-}$endothelial cells. (**a**) Corneal cross-sections prepared from *Nf1* heterozygous and wild-type mice 6 days after bFGF implantation were double immunolabeled for CD31 (endothelial cells) and Ki67 (proliferating cells). Double immunopositive profiles along the vascular tubes were scored and presented as the means (+s.e.; $n=8$) for each genotype (*$P=0.001$, ANOVA). (**b**) BrdU incorporation assay of brain microvessel endothelial cell cultures. *Nf1*$^{+/-}$ and wild-type endothelial cell cultures were treated with a base medium (80% DMEM/F12, 10% horse plasma-derived serum, 10% fetal bovine serum, and 100 μg/ml heparin) or base medium containing either VEGF (50 ng/ml), bFGF (50 ng/ml), or endothelial cell growth supplement (100 μg/ml). Data represent the means (+s.e.) of more than eight replicates for each condition performed in two separate assays on two independent culture preparations.

compared to 7% of their *Nf1*$^{+/-}$ counterparts (Figure 3b). Treatment with endothelial cell growth supplement (a pituitary extract rich in mitogens) increased the BrdU-DNA to 13% for wild-type and 27% for *Nf1*$^{+/-}$ endothelial cultures. VEGF treatment caused a similar but less pronounced differential response. bFGF was a potent mitogen and more than doubled the proliferation of wild-type endothelial cells over that seen in the base medium alone. The response to bFGF by *Nf1*$^{+/-}$ endothelial cells was 3.6-fold greater than in base medium and nearly equaled that with the pituitary growth supplement. Overall, the response of *Nf1*$^{+/-}$ endothelial cells to mitogens was approximately double that exhibited by wild-type cells. These findings indicate that *Nf1* heterozygous endothelial cells had an exaggerated mitogenic response that most likely contributes to the increased angiogenic potential observed in the corneal and retinal assays.

Corneal NV is associated with increased infiltration of inflammatory cells in Nf1$^{+/-}$ *mice*

Next, to test the hypothesis that *Nf1*$^{+/-}$ inflammatory cells might be involved in the increased angiogenic response in *Nf1*$^{+/-}$ mice, we examined the infiltration by macrophages and mast cells in corneal cross-sections adjacent to those used for endothelial cell proliferation assays described above. Mac-1 immunostaining of wild-type corneas showed substantial baseline macrophage infiltration of the corneal and a high macrophage density around the pellet, consistent with observations reported previously (Kenyon *et al*., 1996). Counts of Mac-1 immunopositive cells revealed macrophage infiltration was significantly elevated locally in *Nf1*$^{+/-}$ corneas after bFGF implantation. *Nf1*$^{+/-}$ corneas exhibited a pattern of macrophage infiltration as similar to that in wild-type corneas in avascular area. However, in the NV zone, the number of macrophage was 4.6-fold greater in *Nf1*$^{+/-}$ corneas than wild-type corneas (Figure 4a). The increase in macrophage cell density was most pronounced near the limbal vessels and in general lagged well behind the leading front of the

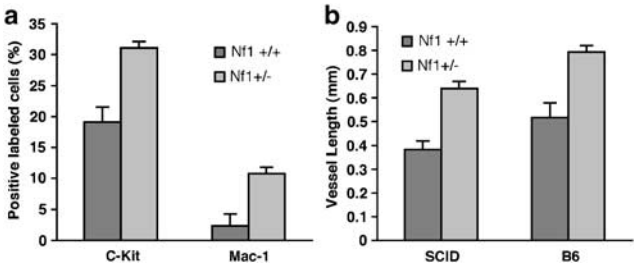

Figure 4 Increased infiltration of inflammatory cells during corneal NV in $Nf1^{+/-}$ mice and reduced corneal NV in $Nf1^{+/-}$*scid* mice. Corneal cross-sections prepared from *Nf1* heterozygous and wild-type mice 6 days after bFGF implantation were immunostained with Mac-1 (macrophages) and c-kit (mast cells) and the percentages of immunopositive cells counted within a defined area. Data represent mean counts (+s.e.) of eight corneas for each genotype (**a**). Corneal flat mounts prepared 6 days after bFGF implantation were immunostained with CD31. The maximum vessel length represent the mean (+s.e.) of four to 13 corneas for each genotype mice (**b**).

growing blood vessels. Similarly, c-Kit immunostaining revealed a 63% increase in mast cell infiltration in the neovascularized area of $Nf1^{+/-}$ corneas compared to wild-type corneas ($P=0.005$, $n=8$) (Figure 4a). In general, the number of inflammatory cells was directly correlated with the amount of NV.

We also examined the effect of *scid* background (T- and B-cell deficiency) on the angiogenic response of $Nf1^{+/-}$ mice by comparing bFGF-induced corneal NV between mice with different genetic backgrounds, including $Nf1^{+/-}$/*scid*, $Nf1^{+/-}$/*B6*, $Nf1^{+/+}$/*scid* and $Nf1^{+/+}$/B6 (Figure 4b). At 6 days after bFGF implantation, the corneal NV in both *scid* and B6 mice were augmented due to $Nf1^{+/-}$ haploinsufficiency (which advanced an average of 0.25 mm for *scid* mice and 0.28 mm for B6 mice). Although the *scid* mice had relatively lower level of corneal NV than B6 mice of the same genotype, the reduction is only statistically significant under the condition of *Nf1* haploinsufficiency ($Nf1^{+/-}$/B6 mice was 24% greater than in $Nf1^{+/-}$/*scid*, $n=4$ and 13, respectively, $P=0.02$). On the other hand, $Nf1^{+/+}$/*scid* and $Nf1^{+/+}$/B6 mice showed no significant difference in their corneal NV ($n=10$ and 13, respectively, $P=0.06$), confirming results reported previously by Kenyon *et al.* (1996). Thus, the reduced corneal NV in $Nf1^{+/-}$/*scid* mice compared to $Nf1^{+/-}$/B6 mice may be due to the lack of haploinsufficient phenotypes of B lymphocytes, which is known to contribute to angiogenic responses in the tumor microenvironment (de Visser *et al.*, 2005). Overall the reduced level of corneal NV due to the *scid* background is limited compared to the effect of *Nf1* haploinsufficiency, suggesting that $Nf1^{+/-}$ B lymphocytes can contribute a minor additive effect to angiogenesis.

Discussion

Transgenic and syngraft studies show that *Nf1* null Schwann cells give rise to neurofibromas in *Nf1* haploinsufficient mice (Zhu *et al.*, 2002; Wu *et al.*, 2005). Although the *Nf1* heterozygous background is also implicated in neurofibroma formation, the underlying mechanisms remain unknown. Given the essential role of angiogenesis in solid tumor growth, we hypothesized that *Nf1* heterozygosity can result in different angiogenic responses to various stimuli, particularly those associated with neurofibroma development. Initially we found that $Nf1^{+/-}$ mice showed a marked increase in hypoxia-induced retinal NV compared to that of wild-type mice. This finding is consistent with a recent report by Ozerdem (2004) using the same neonatal hypoxia model. Additionally, our study showed that there was no significant difference in normal (developmental) retinal NV between $Nf1^{+/-}$ and wild-type mice. Neither study ruled out the possibility that an exaggerated retinal NV in response to ischemia in $Nf1^{+/-}$ mice is mainly a developmental disposition. To that end and to corroborate these findings in a more valid model of NV, we found that adult $Nf1^{+/-}$ mice showed an elevated neovascular response to a single angiogenic factor (bFGF) applied to the cornea. Based on these results we conclude that *Nf1* heterozygosity augments angiogenesis.

Although NF1 is characterized by hyperproliferation and neoplasia of neural crest derivatives, affected individuals often have disorders that seem less related to the neural crest, including hypertension, renal artery stenosis, increased incidence of congenital heart disease, and vascular disorders (Hamilton *et al.*, 2001; Rasmussen *et al.*, 2001; Friedman *et al.*, 2002). As neurofibromin is expressed in blood vessel endothelial and smooth muscle cells, Hamilton and Friedman (2000) suggested that NF1 vasculopathy might result from an alteration of neurofibromin function in these cells. Indeed, transgenic mice with endothelial-specific inactivation of *Nf1* recapitulate key aspects of the complete null phenotype, including multiple cardiovascular abnormalities involving the endocardial cushions and myocardium (Gitler *et al.*, 2003). This phenotype is associated with elevated Ras signaling in $Nf1^{-/-}$ endothelial cells and greater nuclear localization of the transcription factor NFATC1. Similarly, we find that mouse $Nf1^{+/-}$ endothelial cells have an exaggerated response to mitogens *in vitro* and increased migration and proliferation in response to bFGF *in vivo*. This disposition of *Nf1* haploinsufficient endothelial cells surely contributes to the heightened angiogenesis induced by hypoxia and angiogenic factor stimulation we observed, and may also contribute to the NF1 features described above, possibly in association with increased Ras activation.

Macrophage and mast cells, in addition to their role in inflammation, are now recognized as potential epigenetic contributors to cancer and angiogenesis (Coussens and Werb, 2001; Mueller and Fusenig, 2004). In the corneal angiogenesis model, macrophage and mast cell infiltration might occur as part of an inflammatory response caused by the implantation of the bFGF pellet or as part of the angiogenic response to bFGF *per se*. In developing the corneal angiogenesis model, Kenyon *et al.* (1996) sought to exclude

inflammation as an angiogenic stimulus. They documented that the inflammatory cellular activity caused by pellet implantation was minimal and resolved within the first 2 days and prior to any observable NV. This indicates that angiogenesis did not occur as a secondary effect to inflammation and that macrophage and mast cell infiltration was not sustained by bFGF itself. Our studies were in agreement with their observation, indicating that infiltrating macrophages and mast cells appeared not to instigate angiogenesis. This was particularly evident in the exaggerated angiogenic response in *Nf1* haploinsufficient mice, whereby inflammatory cell density was increased but in areas well behind the leading edge of growing blood vessels. We conclude that the infiltration of inflammatory cells is elevated in $Nf1^{+/-}$ corneas and this response is positively correlated with, and likely secondary to, the overall exaggerated angiogenic response.

In tumor development inflammatory cells express a range of proteases and proangiogenic factors including bFGF and VEGF that can promote and sustain tumor progression and angiogenesis. Although the role of macrophages in neurofibroma formation is not characterized, they are more abundant in neurofibromas and MPNSTs than schwannomas (Johnson *et al*., 1989). Also, mast cells show marked infiltration in neurofibromas and have been considered as a major player in neurofibroma formation (Riccardi, 1981; Johnson *et al*., 1989; Ingram *et al*., 2000, 2001). Recent studies showed that $Nf1^{+/-}$ mast cells have increased survival and proliferation, and are hypermotile compared to wild-type cells in response to stem cell factor expressed by $Nf1^{+/-}$ Schwann cells, specifically on $\alpha_4\beta_1$ integrins in response to Kit ligand (KitL) and linked with Ras-class I_A-PI3K-Rac2 pathway. Reintroduction of the GAP-related domain into $Nf1^{+/-}$ mast cell reduces their migration to wild-type levels in response to KitL, providing direct evidence that an $Nf1^{+/-}$ motile phenotype is secondary to hyperactivation of Ras pathway (Ingram *et al*., 2000, 2001; Yang *et al*., 2003).

Loss of *NF1* expression results in impaired neurofibromin-mediated Ras inactivation and leads to increased Ras pathway activation and tumorigenesis. Activation of Ras in Schwann cells derived from $Nf1^{-/-}$ mice and human NF1 tumor has been shown to have increased secretion of soluble factors such as bFGF and KitL (Hirota *et al*., 1993; Mashour *et al*., 2001; Yang *et al*., 2003), which can stimulate proliferation and migration of endothelial and inflammatory cells. Recent studies show that one of the contributions of the stroma to tumor progression is the expression of angiogenic growth factors including VEGF, bFGF, PDGF and others by macrophages, mast cells and other leukocytes. Increased expression of these growth factors is often associated with Ras activation (see review Mueller and Fusenig, 2004). Thus, we can expect that activation of $Nf1^{+/-}$ endothelial cells, mast cells, macrophages and other cell types (e.g. fibroblasts and bone marrow-derived hematopoietic stem cells) that contribute to angiogenesis may have exaggerated expression and response to proangiogenic factors, most likely in association with hyperactivation of Ras. Our studies demonstrate clearly the association of *Nf1* haploinsufficiency in multiple cell types (including inflammatory and endothelial cells) with an exaggerated angiogenic response. These findings may also improve our understanding of the role of haploinsufficiency in angiogenesis and the growth of neurofibroma, leading to possible interventions using antiangiogenic therapies.

Materials and methods

Animals

Our stock colony of *Nf1* knockout mutant mice (*B6*/*Nf1*) (Brannan *et al*., 1994) was produced by in-breeding of mice onto the C57BL/6 background. Mice (*Nf1*/*scid)* with an *Nf1* heterozygous background that were also immunodeficient were generated by cross-breeding B6/*Nf1* and B6/*scid* mice (Wu *et al*., 2005) and are heretofore referred to as *Nf1* mice. The original *scid* mice were obtained from the Jackson Laboratory (Bar Harbor, ME, USA). All methods and animal uses were performed in accordance to the Animal Care and Use Guidelines of the University of Florida College of Medicine.

Genotyping

The *Nf1* locus was genotyped by a 3-oligo system PCR, as described by Brannan *et al*. (1994). The *scid* mutation in the DNA-PKCS gene (a nonsense mutation) was described by Blunt *et al*. (1996). Based on genomic DNA sequence (Genbank AB005213), we developed a PCR-based genotype assay. PCR primers were designed flanking the mutation site in exon 85: *scid* 5′ (GAGTTTTGAGCAGACAATGCTGA) and *scid* 3′ (CTTTTGAACACACACTGATTCTGC). The resulting 180 bp PCR product was digested with Alu I to distinguish wild-type allele (no cut) from mutant allele (cut) via agarose gel electrophoresis, to genotype animals at the *scid* locus.

Endothelial cell culture

Cultures of murine brain microvascular endothelial cells were obtained by modifications of the methods described by Song and Pachter (2003). Briefly, cortical gray matter free of nerves, meninges and choroid plexus was isolated from six 3–5-week-old mice. The cortices were maintained in ice-cold medium and minced into 1 mm pieces. The tissue was homogenized first in a Dounce homogenizer by 30 strokes of a larger clearance pestle ('A' pestle) followed by 25 strokes using the smaller clearance pestle ('B' pestle). The homogenate was centrifuged at 200 *g* for 5 min at 1°C and the supernatant was discarded. The tissue pellet was resuspended in 15 ml of isotonic 18% (wt/vol) dextran solution and centrifuged at 10 000 *g* for 10 min. The tissue pellet was resuspended in 5 ml of Hank's balances salt solution (Ca^{2+} and Mg^{2+} free) and then passed through a 70-μm nylon mesh screen mounted on a syringe barrel. The microvessel fraction retained by the screen was harvested in medium and collected by centrifugation at 200 *g* for 5 min. The microvessels were gently resuspended in 5 ml of Digestion medium containing Hank's, 0.1 U/ml collagenase (type XI, Sigma), 0.8 U/ml Dispase (Collaborative Research), 20 U/ml DNase-1 (Type II-Sterile, Sigma), 0.4 μM tosyl-lysine chloromethyl ketone (Sigma). The mixture was placed in a 60-mm Petri dish and incubated at 37°C in a 5% CO_2/air incubator for 90 min with occasional agitation. By the end of the digestion, endothelial cells start popping out from the vessel fragments, appearing as beads on a string. The digestion should not

proceed to the single-cell level. The partially digested microvessel fragments were collected and resuspended in Growth Medium containing 80% DMEM/F12 (14.3 mM sodium bicarbonate, 20 mM HEPES, pH 7.4), 10% horse plasma-derived serum (Atlanta Biologicals), 10% fetal bovine serum, 100 μg/ml heparin, 100 μg/ml endothelial cell growth supplement (BD Biosciences) and antibiotics. The suspension was seeded onto tissue culture dishes coated with murine collagen IV (50 μg/ml in 0.05 N HCl) (BD Biosciences). The cultures were passaged when confluent by incubating in Hank's solution containing 10 mM EDTA until the cells appeared rounded. The trypsin (0.05%)/EDTA (0.5 mM) was added for 30 s and the cells detached by tapping the dish. The trypsin was neutralized by the addition of medium containing serum and the remaining cells were dislodged by squirting the medium. The suspension was diluted with Growth Medium and passaged 1:5 into collagen IV-coated dishes.

In vitro *proliferation assay*
First passage endothelial cell cultures (5000 cell/well) were seeded into 96-well plates coated with collagen IV and fed a base medium (80% DMEM/F12, 10% horse plasma-derived serum, 10% fetal bovine serum, and 100 μg/ml heparin). After 4 h the cultures were treated with the base medium alone or the base medium containing either endothelial cell growth supplement (100 μg/ml), vascular endothelial cell growth factor (50 ng/ml $VEGF^{165}$, R&D Systems), or basic fibroblast growth factor bFGF (50 ng/ml, R&D Systems). At 24 h after treatments, the medium was brought to 10 μg/ml with bromodeoxyuridine (BrdU) and cultured for an additional 24 h. Fixed cultures were immunolabeled for BrdU-positive DNA and the percentage of cells with BrdU-DNA were scored as described previously (Muir *et al*., 1990).

Induction of angiogenesis by hyperoxia
Mouse pups derived from $Nf1^{+/-}$/*scid* females bred with $Nf1^{+/+}$/*scid* males, with their nursing dam, were placed in a chamber containing 75% oxygen at postnatal day 7 (P7). At 5 days after oxygen treatment, the P12 pups and nursing dam were returned to normal room air and maintained for another 5 days. These pups were terminated at P17 under anesthesia by an overdose of ketamine/xylazine, and their eyes were enucleated and fixed for retinal NV assessment.

Quantification of retinal NV
Retinal NV was scored by methods described by Smith *et al*. (1994). Briefly the enucleated eyes were immersed in 4% paraformaldehyde in PBS for at least 24 h, and embedded in paraffin. Serial sections (5 μm) of whole eyes were cut through the full eyecup parallel to the optic nerve. Representative sections (every 30th section) were stained with hematoxylin and eosin and vascular endothelial cell nuclei outside the internal limiting membrane were counted by trained investigators masked to the identity of each section. Such vascular cell nuclei, on the vitreous side of the internal limiting membrane identified in this protocol, were considered to be associated with NV and provide a reliable evidence for quantitatively assessing the total level of retinal NV in each eye.

Induction of corneal angiogenesis by bFGF micropellets
Young adult mice (8–14 weeks), litters of both $Nf1^{+/-}$/*scid* and $Nf1^{+/+}$/*scid mice*, were anesthetized by intraperitoneal (i.p.) injection of 0.1 ml per 20 g body weight of anesthetic cocktail containing ketamine (12.5 mg/ml) and xylazine (2.5 mg/ml). Both eyes were topically anesthetized with 0.5% proparacaine (Ophthetic, Alcon, TX, USA), and a corneal micropocket (approximately 0.7 mm length) was dissected with a surgical blade and needle (30G1/2) (Sun Surgical). A micropellet ($0.5 \times 0.5 \times 0.2\,mm^3$) of sucralfate and hydron polymer containing bFGF (80 μg or as indicated) was placed into the pocket and advanced to end of the pocket, which extended to within 0.8–1.0 mm of temporal limbus. Antibiotic ointment (erythromycin) (Sun Surgical) was applied postsurgically to the eyes.

Quantification of corneal NV
At 4–6 days after implantation, mice were anesthetized by i.p. injection of ketamine/xylazine mixture. Corneal NV extending from the base of the limbal vascular plexus toward the pellet was measured under standard microscopy (Kenyon *et al*., 1996). Eyes were then enucleated and immersed in 4% paraformaldehyde in PBS for 20 min. Eyes showing any abnormal phenotype such as opacity were excluded from further analysis.

Immunohistochemical staining for vascular endothelial cells was performed on corneal flat mounts. Corneas with part of limbal vascular attached were dissected from enucleated eyes and rinsed with PBS and fixed in 100% acetone for 20 min. After washing in PBS, nonspecific binding was blocked with 0.1 M PBS, 2% albumin for 2 h at room temperature. Corneas were incubated at 4°C for 24 h in primary antibody, fluorescein isothiocyanate-conjugated rat anti-mouse CD31 (FITC-CD31) (BD Pharmingen) diluted 1:500 in blocking buffer. After several washes in PBS at room temperature corneas were mounted on slides and coverslipped with Vectashield (Vector Laboratories Inc., Burlingame, CA, USA). Images of CD31-stained corneal vasculature were captured by confocal fluorescence microscopy. Corneal NV was quantified by measuring the maximum vessel length extending from the base of the limbal vascular plexus toward the pellet and the maximum contiguous circumference along the base of the limbal of NV zone using Image-Pro Plus software.

Immunolabeling corneal vasculature
After flat-mount examination of corneal NV, corneas were cryo-sectioned (10 μm) parallel to the center of neovasculature zone and implanted pellet. Every 10th was stained with Hoechst solution (1:100) (Sigma) to localize nuclei. Sections which showed increased cellularity and pellet material were selected for more detailed immunohistochemical staining. Sections were rinsed, blocked and permeablized, and incubated with one of the following primary antibodies: FITC-CD31, mouse anti-human Ki-67 (BD Pharmingen), c-kit (Santa Cruz, sc-168), or mac-1 (BD Pharmingen). Bound antibodies were labeled with goat anti-mouse-Alexa Fluor 568 (Molecular Probes) or peroxidase-conjugated secondary antibodies followed by chromogenic development. For all immunohistochemical stains, sections without addition of primary antibodies served as negative controls. Endothelial cell proliferation was assessed in corneal cross-sections double-labeled for CD31 (endothelial cells) and Ki-67 (a proliferation marker). Double-labeled profiles were scored using Image-Pro Plus software. Single factor analysis of variance was used for statistical analysis of the data obtained from eyes of *Nf1* heterozygous and wild-type mice.

Acknowledgements

We thank Drs William Hauswirth and Maria Grant for guidance in developing the retinal NV model. Elizabeth Baldwin, Hua Li, Fredrick Kweh and Debbie Neubauer,

provided excellent technical assistance. This work was supported by US Army Neurofibromatosis Research Program Grants DAMD170310224 (DM) and DAMD170110707 (MRW).

References

Arbiser JL, Flynn E, Barnhill RL. (1998). *J Am Acad Dermatol* **38**: 950–954.
Bajenaru ML, Hernandez MR, Perry A, Zhu Y, Parada LF, Garbow JR *et al*. (2003). *Cancer Res* **63**: 8573–8577.
Ballester R, Marchuk D, Boguski M, Saulino A, Letcher R, Wigler M *et al*. (1990). *Cell* **63**: 851–859.
Blunt T, Gell D, Fox M, Taccioli GE, Lehmann AR, Jackson SP *et al*. (1996). *Proc Natl Acad Sci USA* **93**: 10285–10290.
Brannan CI, Perkins AS, Vogel KS, Ratner N, Nordlund ML, Reid SW *et al*. (1994). *Genes Dev* **8**: 1019–1029.
Coussens LM, Werb Z. (2001). *J Exp Med* **193**: F23–F26.
de Visser KE, Korets LV, Coussens LM. (2005). *Cancer Cell* **7**: 411–423.
Duprez K, Bour C, Merle M, Duprez A. (1991). *Microsurgery* **12**: 1–8.
Friedman JM, Arbiser J, Epstein JA, Gutmann DH, Huot SJ, Lin AE *et al*. (2002). *Genet Med* **4**: 105–111.
Gitler AD, Zhu Y, Ismat FA, Lu MM, Yamauchi Y, Parada LF *et al*. (2003). *Nat Genet* **33**: 75–79.
Hamilton SJ, Allard MF, Friedman JM. (2001). *Am J Med Genet* **100**: 95–99.
Hamilton SJ, Friedman JM. (2000). *Clin Genet* **58**: 341–344.
Hirota S, Nomura S, Asada H, Ito A, Morii E, Kitamura Y. (1993). *Arch Pathol Lab Med* **117**: 996–999.
Ingram DA, Hiatt K, King AJ, Fisher L, Shivakumar R, Derstine C *et al*. (2001). *J Exp Med* **194**: 57–69.
Ingram DA, Yang FC, Travers JB, Wenning MJ, Hiatt K, New S *et al*. (2000). *J Exp Med* **191**: 181–188.
Johnson MD, Kamso-Pratt J, Federspiel CF, Whetsell Jr WO. (1989). *Arch Pathol Lab Med* **113**: 1263–1270.
Kenyon BM, Voest EE, Chen CC, Flynn E, Folkman J, D'Amato RJ. (1996). *Invest Ophthalmol Vis Sci* **37**: 1625–1632.
Kim HA, Ling B, Ratner N. (1997). *Mol Cell Biol* **17**: 862–872.
Mashour GA, Ratner N, Khan GA, Wang HL, Martuza RL, Kurtz A. (2001). *Oncogene* **20**: 97–105.
Mashour GA, Wang HL, Cabal-Manzano R, Wellstein A, Martuza RL, Kurtz A. (1999). *J Invest Dermatol* **113**: 398–402.
Morello F, Shah P, Dowling K, Siskin G. (2001). *J Vasc Interv Radiol* **12**: 773–774.
Mueller MM, Fusenig NE. (2004). *Nat Rev Cancer* **4**: 839–849.
Muir D, Varon S, Manthorpe M. (1990). *Anal Biochem* **185**: 377–382.
Ozerdem U. (2004). *Angiogenesis* **7**: 307–311.
Raisler BJ, Berns KI, Grant MB, Beliaev D, Hauswirth WW. (2002). *Proc Natl Acad Sci USA* **99**: 8909–8914.
Rasmussen SA, Yang Q, Friedman JM. (2001). *Am J Hum Genet* **68**: 1110–1118.
Riccardi VM. (1981). *Birth Defects: Original Article Series*, Vol. 17. In: Blandau R, Paul N, Dickman F (eds). Alan R. Lis Inc.: New York, pp. 129–145.
Sheela S, Riccardi VM, Ratner N. (1990). *J Cell Biol* **111**: 645–653.
Side L, Shannon K. (1998). *Neurofibromatosis type 1*. Bios Scientific Publishers Ltd.: Oxford, United Kingdom.
Smith LE, Wesolowski E, McLellan A, Kostyk SK, D'Amato R, Sullivan R *et al*. (1994). *Invest Ophthalmol Vis Sci* **35**: 101–111.
Song L, Pachter JS. (2003). *In vitro Cell Dev Biol Anim* **39**: 313–320.
Wolkenstein P, Mitrofanoff M, Lantieri L, Zeller J, Wechsler J, Boui M *et al*. (2001). *Arch Dermatol* **137**: 233–234.
Wu M, Wallace MR, Muir D. (2005). *J Neurosci Res* **82**: 357–367.
Xu GF, O'Connell P, Viskochil D, Cawthon R, Robertson M, Culver M *et al*. (1990). *Cell* **62**: 599–608.
Yang FC, Ingram DA, Chen S, Hingtgen CM, Ratner N, Monk KR *et al*. (2003). *J Clin Invest* **112**: 1851–1861.
Zhu Y, Ghosh P, Charnay P, Burns DK, Parada LF. (2002). *Science* **296**: 920–922.

In Vitro Studies of Steroid Hormones in Neurofibromatosis 1 Tumors and Schwann Cells

Lauren Fishbein[1,2], Xuelian Zhang[1], Lori B. Fisher[1], Hua Li[1], Martha Campbell-Thompson[3,6], Anthony Yachnis[3,6], Allan Rubenstein[4], David Muir[5,6], Margaret R. Wallace[1,6,7]

[1]Molecular Genetics and Microbiology, UF College of Medicine, Gainesville, Florida
[2]University of Florida College of Medicine Interdisciplinary Program in Biomedical Sciences, Gainesville, Florida
[3]Pathology, Immunology and Laboratory Medicine, University of Florida College of Medicine, Gainesville, Florida
[4]NexGenix Pharmaceuticals, New York, New York
[5]Pediatrics, Division of Neurology, and Department of Neuroscience, University of Florida, Gainesville, Florida
[6]University of Florida McKnight Brain Institute and University of Florida Shands Cancer Center, Gainesville, Florida
[7]Pediatrics, Division of Genetics, University of Florida, Gainesville, Florida

Corresponding author: Margaret R. Wallace
University of Florida
Department of Molecular Genetics
PO Box 100266
Gainesville, FL 32610-0266
Phone: 352-392-3055
Fax: 352-846-2042

Grant support: This work was supported by US Army NF Program grants DAMD 170110707 (MRW) and DAMD 170010549 (DM), the Hayward Foundation, and an NIH NRSA fellowship 1 F30 NS43951 (LF).

Abbreviations

AI apoptosis index
ANOVA analysis of variance
AR androgen receptor
BrdU bromodeoxyuridine
DAB 3,3-diaminobenzidine
EGFR epidermal growth factor receptor
ER estrogen receptor
ERBB2 HER2/neu
HPRT hypoxanthine phosphoribosyl transferase
MPNST malignant peripheral nerve sheath tumor
NF1 neurofibromatosis 1
PCR polymerase chain reaction
PI proliferation index
PR progesterone receptor
SERM selective estrogen receptor modulator
VEGF vascular endothelial growth factor

Running Title: Steroid Hormones in NF1

Key Words: NF1, steroid hormone receptors, Schwann cell, neurofibroma, apoptosis

Abstract

The most common NF1 feature is the benign neurofibroma, which consists predominantly of Schwann cells. Dermal neurofibromas usually arise during puberty and increase in number throughout adulthood. Plexiform neurofibromas, associated with larger nerves, are often congenital and can be life-threatening. Malignant peripheral nerve sheath tumors in NF1 are believed to arise from plexiforms in 5-10% of patients. There are reports of increased potential for malignant transformation of plexiform tumors, and increase in dermal neurofibromas, during pregnancy. These observations suggest that steroid hormones influence neurofibroma growth, and our work is the first to examine steroid hormone receptor expression and ligand-mediated cell growth and survival in normal human Schwann cells and neurofibroma-derived Schwann cell cultures. Immunohistochemistry and real-time PCR showed that estrogen receptors, progesterone receptor and androgen receptor are differentially expressed in primary neurofibromas and in NF1 tumor-derived Schwann cell cultures compared to normal Schwann cells. However, there is substantial heterogeneity, with no clear divisions based on tumor type or gender. The *in vitro* effects of steroid hormone receptor ligands on proliferation and apoptosis of early passage NF1 tumor-derived Schwann cell cultures were compared to normal Schwann cell cultures. Some statistically significant changes in proliferation and apoptosis were found, also showing heterogeneity across groups and ligands. Overall, the changes are consistent with increased cell accumulation. Our data suggest that steroid hormones can directly influence neurofibroma initiation or progression by acting through their cognate receptor, but that these effects may only apply to a subset of tumors, in either gender.

Introduction

Neurofibromatosis 1 (NF1) is an autosomal dominant disorder which affects about 1 in 3500 individuals worldwide. The NF1 tumor suppressor gene is located on chromosome 17q11.2 [1, 2, 3]. Despite full penetrance of the disease, there is variable expressivity seen even within families with the same constitutional mutation. The most characteristic feature of NF1 is the neurofibroma. Dermal (cutaneous and subcutaneous) neurofibromas are often size-limited and are mainly of cosmetic significance. Interestingly, these tumors often first develop during puberty and continue to increase in number throughout life. The plexiform neurofibromas form along deeper nerves in the body; and although they are slow-growing, they can become large and even life threatening. Nevertheless, many patients have internal plexiform tumors which are asymptomatic. In addition, there is a 5-10% chance of malignant potential for the plexiform tumors to become malignant peripheral nerve sheath tumors (MPNSTs). Many plexiform tumors are thought to be congenital. Some patients have reported an increase in size and number of both dermal and plexiform neurofibromas during pregnancy [4] or while taking birth control pills (Wallace, unpublished data). A recent survey of 59 NF1 patients found that oral contraceptive pills did not stimulate subjective growth of neurofibromas in the majority of patients, in contrast to two patients receiving high dose depot contraceptive with progesterone who did report significant tumor growth [5]. There have even been reports of increased malignant potential of plexiform tumors during pregnancy [6, 7]. This information suggests that steroid hormones may play a role in neurofibroma development, growth and/or survival.

Neurofibromas are heterogeneous, consisting of fibroblasts, mast cells, perineural cells and a majority of Schwann cells (some of which are clonally derived with somatic NF1 mutations). Nuclear steroid hormone receptors commonly regulate transcription of genes involved in the cell proliferation and apoptosis pathways, although this has never been tested in

Schwann cells. Little research has been done on steroid hormone effects on Schwann cells. Jung-Testas et al. found low levels of estrogen receptor (ER) on cultured rat Schwann cells using binding assays [8]. These cells showed a proliferative response to estradiol but only in the presence of forskolin, suggesting that increased cAMP is required for the effect. The same group demonstrated the presence of progesterone receptor (PR) in rat Schwann cells using ligand binding assays and receptor immunofluorescence [9]. In addition, PR is known to have a role in glial cells in activating genes involved in myelin production [10, 11]. Interestingly, estrogen treatment had no effect on PR level [12], in contrast to reciprocal regulation observed in reproductive organs of the rat. Furthermore, estrogen treatment of these cells did not increase ER binding or immunofluorescence. Another study examined estrogen and progesterone responsiveness in cultured Schwann cells derived from various aged rodents, and found that high levels of 17β-estradiol and progesterone had small proliferative effects in Schwann cells from males and newborns only [13].

While steroid hormones are involved in a number of tumors (e.g. breast and ovarian carcinoma, prostate carcinoma and benign meningiomas), little work has been done to analyze the effects of steroid hormone receptors in human Schwann cell tumors. Martuza et al. found evidence of ERs in schwannomas, but only in 1 of 6 neurofibromas, via ligand binding assays of dissociated tumor cells [14]. There was no progestin binding in 2 of 2 neurofibromas. Furthermore, Chaudhuri et al. failed to show any ER or PR binding in 5 neurofibromas and 4 neurofibrosarcomas [15]. A more recent study found PR immunoreactivity in some unidentified cells within human neurofibroma tissue sections (apparently not Schwann cells) but found no significant ER immunostaining [16]. Thus far, no human neurofibromas or MPNSTs have been studied *in vivo* or *in vitro* for transcript levels of *ER* and *PR*, or cellular response to the steroid hormones.

Overall, the literature suggests that ER and PR might be present in human Schwann cells, but the status of these in NF1-related neurofibromas is essentially unknown. Due to the limited and somewhat conflicting data reported in the literature, it is unclear if or how human Schwann cells (normal or neurofibroma-derived) respond to steroid hormones. Based on the clinical data suggesting that neurofibromas are aggravated in some patients during times of hormonal surges, we hypothesized that steroid hormone receptors would be differentially expressed in NF1 neurofibromas and that neurofibroma-derived Schwann cells would have an altered sensitivity to ligands for these receptors, compared to normal (non-NF1) Schwann cells. Here we describe the first molecular study of the presence of steroid receptors and effects of their agonists/antagonists at the cellular level in neurofibroma-derived and normal Schwann cells.

Materials and Methods

Sample Collection and Total Cellular RNA Isolation

Sample collection was completed with approval by the University of Florida IRB. Most of the primary tumor and tumor-derived Schwann cell cultures were from patients who met diagnostic criteria for NF1 [18], although a few were sporadic neurofibromas. Histologically, the primary samples contained ≥70% Schwann cells (fibroblasts, mast cells, nerve axons, perineural cells and vascular endothelial cells making up the rest), and the tumor-derived Schwann cell cultures were enriched to >95% purity with neuregulin. Normal (non-NF1) and neurofibroma Schwann cells were cultured and enriched from primary tissue as previously described [17]. The cultures utilized were the first Schwann cell enriched passages available (usually passage number 3 to 6), as earlier passages contained other cell types in excess. Therefore, the tumor-derived Schwann cell enriched cultures were not long-term immortal cultures, but rather short-term cultures enriched for the Schwann cell population. The malignant peripheral nerve sheath (MPNST) cultures were the only immortal cultures since they were

derived from malignant tumors. RNA isolation from cultured cells and primary tissue was performed using TRIzol (Invitrogen, Carlsbad, CA). The positive control samples included Caco-2 (ERα-/ERβ+ human colon cancer cell line [19]), MCF-7 (ERα+/ERβ-/PR+ human breast cancer cell line [20]), and human testis RNA (AR+ [21]).

Real-Time PCR

Reverse transcription reactions of 2μg of total RNA used random hexamers and Superscript II (Invitrogen, Carlsbad, CA) in a 20μl volume. Diluted (1:5) cDNA (1μl) was used as a template in a LightCycler rapid real-time thermal cycler system (Roche, Indianapolis, IN) as follows: 10 mins. at 95°C, then cycling for 5 secs. at 94°C, 5 secs. at primer specific annealing temperature, 30 secs. at 72°C for 48 cycles in a 10μl volume using the Fast Start DNA Master SYBR GreenI mix (Roche, Indianapolis, IN). Fluorescent product was detected at the end of each extension step. Primer sequences are listed in Table 1 and were designed to span at least one large intron. A melting curve analysis and native polyacrylamide gel electrophoresis were performed for each reaction to confirm amplification specificity. A standard curve was generated by amplifying serial dilutions of a purified PCR product specific for each gene of interest. The data points were transformed to a log format and a linear regression line y=ax+b with a slope in the range of –2.9 to –4 was used to determine values for each sample. Calculated values were then taken as a ratio compared to the average value from two separate normal Schwann cell culture samples, as Schwann cells are the predominate cell type in neurofibromas (≥70%). All reactions were repeated in duplicate and normalized to *HPRT* gene expression (a housekeeping gene commonly used as a control in such experiments, including in neuronal tissue [22]). Furthermore, each sample set was run with a positive and negative control sample from MCF-7, Caco-2 or testis cells depending on the gene being analyzed.

Progesterone Receptor and c-kit Immunohistochemistry

Seventy-one formalin-fixed paraffin-embedded human neurofibroma sections (8μm) were stained with the monoclonal anti-progesterone receptor antibody (DAKO, Carpinteria, CA; Clone PgR 636, 1:50). Positive control slides of PR+ breast carcinoma tissue were used. Endogenous peroxidase activity was blocked with 1% hydrogen peroxide, and the sections were heated at 95°C for 30 mins in antigen retrieval buffer (DAKO, Carpinteria, CA) to unmask receptor epitopes. The antibodies were detected with a biotinylated goat anti-mouse secondary antibody (DAKO, Carpinteria, CA; 1:500) and ABC kit (DAKO, Carpinteria, CA), using 3,3-diaminobenzidine (DAB) (Sigma, St. Louis, MO) as a substrate. Data were analyzed using the methods described in McLaughlin and Jacks [16] to determine amount of PR immunoreactivity. Briefly, tumors were classified as negative if less than 5 positive cells were seen per 10 high power fields, rare positive if 5 to 20 positive cells were seen per 10 high power fields, focal positive if greater than 20 positive cells were seen per 10 high power fields and diffusely positive if positive cells were easily seen throughout the tissue sample.

Double staining was performed for PR and c-kit (a mast cell marker) using fluorescent antibodies. The procedure was the same as described above with the monoclonal anti-progesterone receptor antibody (DAKO, Carpinteria, CA; Clone PgR 636 1:25) and the polyclonal anti-c-kit antibody (Santa Cruz Biotechnology, Santa Cruz, CA; Clone C-19 1:50). The antibodies were detected using a fluorescent labeled secondary goat anti-rabbit (Invitrogen, Carlsbad, CA; 1:300) for c-kit and goat anti-mouse (Invitrogen, Carlsbad, CA; 1:300) for PR.

Proliferation and TUNEL Assays

Normal human Schwann cells and neurofibroma-derived Schwann cell cultures were grown as previously described [17]. The cells were trypsinized, neutralized with serum-containing medium, and washed in phenol red free DMEM. The cells were then plated and incubated for 48 hours in phenol red free DMEM with 1% dextran-coated charcoal-treated fetal

bovine serum. Then, for three days cells were treated in replicate chambers with ethanol carrier alone, 100nM 17ß-estradiol or progesterone (agonists for ER and PR, respectively), or 1μM ICI 182,780 (antagonist for ER), tamoxifen (mixed ER agonist/antagonist, SERM), or mifepristone (antagonist for PR) (Sigma, St. Louis, MO). These concentrations were chosen based on literature providing physiological levels for analysis of hormone effects. Cells for the proliferation assay were treated with 1μM BrdU (Sigma, St. Louis, MO) added for the final 24 hours and then fixed in 70% EtOH for 30 mins. at 4°C. Immunohistochemistry was completed on these cells using a mouse anti-BrdU primary antibody (DAKO, Carpinteria, CA; 1:200) and a secondary goat anti-mouse HRP antibody (DAKO, Carpinteria, CA; 1:500) and visualized with DAB (Sigma, St. Louis, MO). Cells used for the TUNEL assay were fixed in 4% paraformaldehyde for 25 mins. at room temperature, and immunohistochemistry was completed using the Promega DeadEnd Colorimentric Kit (Madison, WI). Assays were done in replicate, and pictures of the slides from both assays were taken under a microscope with 200X magnification. Eight pictures were taken in a linear fashion across each chamber. Proliferation and apoptosis indices (PI or AI) are reported as a percent of cells which were stained.

Downstream Gene Expression Analysis

For each culture, a standard regimen was used. The cells were treated (after the 48 hour washout period) on day 0, 3 and 6 with 100nM 17ß-estradiol or progesterone or ethanol carrier alone in replicate wells. The cells were harvested for RNA on day 0, 1, 3 and 7 to be used in real-time PCR analysis for expression of putative downstream targets of steroid hormone receptors (including *ERα, ERβ, PR*, *ERBB2*, *EGFR* and *VEGF*) as described above. The samples were normalized to *HPRT* and calculated values were taken as a ratio of the hormone treated sample compared to the same culture on day 0 before hormone treatment. For some cultures, RNA collection was only done on days 0, 1 and 3 due to an inadequate number of cells.

Statistics

Real-time PCR data were analyzed by one-way analysis of variance (ANOVA) followed by Tukey's post-test analysis (GraphPad Prism software, San Diego, CA), to test for significant differences in expression for each gene between the tumor types.

Proliferation and apoptosis rates were analyzed using a one-way ANOVA followed by a Dunnett's post-test analysis (GraphPad Prism software, San Diego, CA) for comparison between control and experimental treatments within each culture. The percentage of stained cells from each picture per treatment was considered as an individual data entry point (n=32; 8 pictures per chamber/ 2 chambers per replicate). For other analyses, the average percent of stained cells from each replicate assay was counted as a data entry point (n=2). For all of these analyses, data points were entered as percent of stained cells and also as a percent change from the average of the no-treatment control's PI or AI for each culture. Additional one-way ANOVA analysis was performed to determine any significant differences between proliferation or apoptosis within each class of tumor cultures compared to the normal Schwann cells for each treatment. A standard $p \leq 0.05$ was used to determine statistical significance. Finally, "trends" in proliferation and apoptosis for each treatment were reported for changes greater than or equal to 10% of the average no-treatment control value for each culture (but not meeting statistical significance), using n=2 as described above.

Results

Steroid Hormone Receptors are Present in Normal Schwann Cells and Most Tumor Samples

Two independent normal Schwann cell cultures, pn97.3 and pn97.4, were analyzed for RNA expression of the *ERα*, *ERβ*, *PR* and *AR* genes. The tumor samples analyzed were grouped as follows (with some tumors having both primary and culture samples): 17 primary dermal

neurofibromas and 8 dermal tumor-derived Schwann cell cultures, 10 primary plexiform neurofibromas and 10 plexiform tumor-derived Schwann cell cultures, and 2 primary MPNSTs and 2 MPNST tumor-derived Schwann cell cultures. The results are shown in Table 2, and the values are normalized based on the average of the normal Schwann cells. Normal Schwann cell cultures were used for the comparison because Schwann cells are the principal cell type in the tumor cultures (>95%) and in the solid tumors (≥70%).

Tumors Show Different Levels of *ERβ*, *PR* and *AR*

Most samples had detectable expression of all four genes. Many tumor samples had differential expression (change of 10-90%) compared to normal Schwann cell cultures, consistent with our hypothesis, with the largest differences seen in primary tumor RNAs. In fact, when examining differences between tumor types for expression of each gene, *ERβ*, *PR* and *AR* showed statistically significant differences ($p<0.05$ with one-way ANOVA), but there was greater variation between primary versus culture samples than between tumor type. Thus, the expression data did not stratify the types of neurofibromas, but rather may imply that hormone receptor expression can be found in cell types other than the Schwann cell. For *ERβ*, the expression was undetectable in most of the culture samples, whereas the primary tissue samples had expression often equal to that in the normal Schwann cell cultures. For *PR*, the expression was significantly ($p<0.05$) increased in the primary tissue sections from dermal and plexiform tumors compared to the tumor cultures (which showed expression levels similar to the normal cultures). The primary MPNST samples also had an increase in *PR* expression although it did not reach statistical significance. *AR* expression was significantly ($p<0.05$) increased in dermal and plexiform primary tissue samples compared to dermal and plexiform cultures. Although the MPNST samples did not show statistical significance, the cultures had higher expression compared to the primary tissue samples.

Overall, *PR* seemed to have the largest differential expression within these samples (30-90% increase for most), and it was typically greater than normal, with 9 samples being as high or higher than the positive control (MCF-7) compared to normal Schwann cells. Lastly, no obvious relationship between patient gender and expression levels of receptors was seen in any tumor type.

PR Immunohistochemistry

To follow up the *PR* RNA results, histological sections from 71 neurofibromas (38 dermal, 29 plexiform and 4 MPNSTs) were immunostained for PR. Interestingly, half of the women contributing tumors to this immunohistochemical analysis reported neurofibroma growth in response to pregnancy or birth control pills. Overall, there was no obvious correlation with PR positive sections and gender, hormone-response or family history of NF1, type of tumor, or location of tumor. Of the 71 tumors, 54% were positive for PR compared to 75% reported in the literature [16] (Figure 1). Of the PR positive tumors, 45% had diffuse staining, 37% had focal positive staining and 16% had rare positive staining (as described in materials and methods). The positive samples were derived from 14 female and 7 male patients and included 1 MPNST, 25 dermal neurofibromas and 12 plexiforms (2 of which were sporadic isolated neurofibromas in individuals otherwise not meeting NF1 criteria).

Of the 38 positive samples, 8 were tested in the real-time PCR analysis as well. Interestingly, 7 of the 8 tumors showed an increase in *PR* RNA expression for either the primary and/or culture samples (UF 17T1, UF 17T2, UF 505T7, UF 378T, UF 537T1, UF 328T7, and UF 505T3), with the primary sample always having higher differential expression than the tumor-derived Schwann cell culture data, if both were available. This suggests that the increased transcription correlates with an increase in expression at the protein level and that the positive cells are not necessarily of Schwann cell origin. To further examine the cell of origin for

positive PR staining, the c-kit antibody was used as a marker for mast cells. Double immunostaining for PR and c-kit on two PR+ samples demonstrated that the mast cells were not expressing the PR (data not shown).

Interestingly, all five dermal neurofibromas from a pregnant NF1 subject were negative, but all three dermal neurofibromas from this same patient removed postpartum showed diffuse positive staining. This suggests heterogeneity and/or transient expression of these markers perhaps in response to hormonal changes consistent with a previous report [16]. ERα and ERβ immunohistochemistry was performed on 10-15 neurofibroma sections, all of which showed no reactivity (UF Shands Clinical Pathology Lab Core, data not shown).

Proliferation and TUNEL Assays Show Heterogeneous Results

Functional assays of 19 samples tested the hypothesis that early passage neurofibroma-derived Schwann cells have an altered sensitivity to steroid hormones. Four normal Schwann cell cultures, 7 plexiform-derived Schwann cell cultures, 6 dermal-derived Schwann cell cultures and 2 MPNST-derived Schwann cell cultures were analyzed for effects of steroid hormones on growth and survival. Figure 2 shows examples of cultures after the TUNEL assay (to measure apoptosis) and after staining for BrdU incorporation (to measure proliferation).

The proliferation and apoptosis results are reported as the percent change to reflect alterations seen in cells with treatment relative to the same culture without treatment. Within each culture, proliferation index (PI) and apoptotic index (AI) differences due to treatment were examined with a one-way ANOVA (n=32). Overall, out of 19 cultures there were 7 statistically significant differences in proliferation or apoptosis associated with the receptor ligand treatments. These changes are summarized in Table 3 and described below.

ICI 182,780, an ER antagonist, decreased proliferation ($p<0.05$) in two cultures (both female): a normal Schwann cell culture (pn02.3) and a dermal neurofibroma-derived Schwann

cell culture (cNF99.1). Tamoxifen, a SERM, caused a decrease in proliferation ($p<0.05$) in two cultures: the same normal Schwann cell culture (pn02.3) and a male plexiform neurofibroma-derived Schwann cell culture (pNF00.11). Tamoxifen also increased proliferation ($p<0.05$) in the female plexiform culture pNF00.13. Lastly, mifepristone, typically a PR antagonist, increased proliferation ($p<0.05$) in the male dermal culture cNF97.5. When analyzing apoptotic indices, only one plexiform culture showed a statistically significant response (17β-estradiol increased apoptosis ($p<0.05$) in the female culture pNF99.5). Cultures which have a statistically significant response to a specific treatment did not necessarily show a corresponding increase in receptor RNA expression in the real-time PCR profile. For example, the dermal neurofibroma-derived culture cNF97.5 had no detectable *PR* expression, although this culture demonstrated an increase in proliferation with mifepristone treatment. There is precedent for this situation in the literature as tamoxifen, for example, has been shown to inhibit proliferation and induce apoptosis in ovarian cancer cell lines negative for ER [23, 24].

Tables 4 and 5 display the results from the proliferation and apoptosis assays for cultures which show changes in PI and AI, respectively, by more than 10% compared to the no-treatment control. With this analysis, some trends were found in all tumor types and both genders despite the lack of statistical significance. For example, 3 of 6 dermal cultures displayed increases in proliferation in response to mifepristone, and 3 of 7 plexiform cultures showed decreases in response to tamoxifen. Interestingly, some cultures showed an increase in proliferation with 17β-estradiol and a corresponding response to the SERM tamoxifen, either an increase (pNF02.6-female) or decrease (pn97.4-male) in proliferation. Similarly, progesterone increased proliferation in the female culture cNF96.5f, while mifepristone caused a decrease in the same culture. Also in cNF96.5f, progesterone was related to a trend toward increased proliferation and decreased apoptosis, as was mifepristone in cNF98.4d (male culture). This pattern is consistent

with cell accumulation in the presence of these ligands. All of the average PIs (regardless of treatment conditions) for the normal Schwann cells as well as the dermal and plexiform cultures were within the range of 1-33% (median: 4.5%, 7.7%, and 9.7%, respectively), while the MPNST cultures ranged from 37-67% (median: 54.0%).

Only one plexiform culture with one treatment (pNF00.11/mifepristone) showed a decrease in apoptosis; all other significant changes or trends were toward increased apoptosis in the presence of ligand. Although many cultures showed at least a 10% change in AI in response to various ligands, it must be noted that all the average apoptotic rates (normal and tumor-derived) were under 7% (with most below 5%). Neither MPNST culture (both male) showed a significant increase (or trend) in proliferation in response to any of the ligands, probably due to the already extremely high PI for these malignant cultures; however, they both showed increased apoptosis. This could be an interesting observation for future therapeutic research. There were no trends or significant outcomes that seemed related to patient gender.

A final analysis examined effects from treatments on tumor type using a one-way ANOVA. This analysis found that the treatments did not affect one tumor group more than another for either PI or AI, although the MPNST cultures consistently had a statistically significantly higher PI regardless of treatment condition ($p<0.05$), as expected due to their malignant nature.

Downstream Gene Expression Analysis

Functional effects of steroid hormones in the cell can also be tested by assaying changes in transcription levels of downstream target genes of the receptors. Since downstream targets are not known for Schwann cells, six genes of interest which are known to be affected in other cell types were chosen for analysis. However, real-time PCR results showed no significant alterations in expression of three of the six genes, *ERBB2*, *EGFR* or *VEGF,* in any of the cell

cultures under any treatment conditions (two cultures were not tested due to an inadequate number of cells, pn02.7 and pNF02.6; data not shown). In some samples, the three other genes, *ERα, ERβ,* and *PR,* had RNA level alterations compared to day 0 untreated cells. However, these changes were often paralleled by an equal change in the untreated cells at the corresponding time point, making the interpretation difficult and suggesting that the changes in expression were not due to treatment but rather to time spent in culture. Nevertheless, data from a few cultures showed alterations in expression, which are not seen in the untreated cells at those time points (data not shown). Three female cultures (normal Schwann cell culture pn02.3, dermal culture cNF99.1 and plexiform culture pNF00.13) showed an increase in *ERα* RNA expression after 3 or 7 days of treatment with 17β-estradiol (change compared to untreated cells of 40%, 20%, and 20%, respectively). Interestingly, these cultures showed statistically significant changes in proliferation (decrease, decrease, increase, respectively) in response to ER ligands (ICI 182,780 and/or tamoxifen) (Table 3). Progesterone treatment also increased *ERα* expression in pn02.3 and cNF99.1 (change compared to untreated cells of 20% for both cultures). After one day of treatment, progesterone caused a decrease in *ERα* expression to undetectable levels in the female plexiform culture pNF99.5, which was sustained across the 7 days of the assay. This culture was the only sample to show a statistically significant increase in apoptosis with 17β-estradiol treatment (Table 3). The male plexiform culture pNF95.6, showed a decrease in *ERα* expression to undetectable levels with both 17β-estradiol and progesterone, but only after 7 days of treatment. Finally, the male dermal culture cNF97.5 showed a transient decrease in *PR* expression to undetectable levels after one day of treatment with progesterone. The level returned to that of the untreated cells by day 3.

Discussion

This is the first study to examine steroid hormone receptor expression at the RNA level in human neurofibromas, normal Schwann cell cultures, and neurofibroma-derived enriched Schwann cell cultures. This study also reports the first analysis of proliferative and apoptotic response of such Schwann cell cultures to steroid hormones and their antagonists. Some significant, but heterogenous, results were found, as discussed below.

Steroid Hormone Receptor and Downstream Gene Profile

Characterization of the steroid hormone receptor profile in primary neurofibromas and tumor-derived Schwann cell cultures showed expression of *ERα*, *ERβ*, *PR* and *AR* RNA in most samples, with corresponding PR immunostaining in 7 of 8 neurofibromas tested in both analyses. Among 71 neurofibromas, 54% showed PR positive immunostaining. Together, these data suggest that multiple cell types in the primary neurofibroma together contribute to the steroid hormone RNA expression. Our data are consistent with a study showing that PR immunohistochemical staining is found in cells which express neurofibromin and do not express S-100, suggesting that PR expression is much less in the clonal Schwann cell population [16] but is not in mast cells. The fact that *ERα* and *ERβ* had lower differential RNA expression across the tumor panel is consistent with the finding that ER immunostaining is negative in neurofibroma tissue sections (data not shown and [16]). Thus, although *ERα* and *ERβ* transcripts are present at low levels in tumor samples compared to normal Schwann cells, the protein is undetectable via immunostaining. This may also be consistent with a lack of expression alteration of six putative downstream gene targets. *EGFR* was chosen because it can be regulated by ERα expression [25], and EGFR expression has been seen in distinct foci with immunohistochemistry on neurofibroma sections [26]. *ERBB2* is an oncogene regulated via ER in many cell types, and dimerizes with ERBB3 in Schwann cells [27] to bind neuregulin, a potent mitogen for Schwann cells. Interestingly, overexpression of *ERBB2* can transform Schwann cells [28], and ENU-treated

rodents develop neurofibromas with *ERBB2* activating point mutations [29]. *VEGF* is a target gene for ER in breast cancer cell lines, while estradiol-induced VEGF expression depends on ER subtype and homo- or heterodimerization [20]. This was chosen since neurofibromas can be highly vascular tumors. In addition, estrogen and progesterone can regulate the expression of their own and each others receptors in other cell types. However, real-time PCR analysis of these six genes' transcripts showed negligible alteration in most of the neurofibroma-derived Schwann cell cultures after treatment with 17β-estradiol or progesterone, suggesting that these genes may not be regulated by ER and/or PR in Schwann cells, or that effects are subtle and heterogeneous.

Proliferation and Apoptosis Assays

Despite heterogeneity, even within normal Schwann cells, some statistically significant differences were seen in the rate of proliferation or apoptosis of untreated cells compared to hormone receptor ligand treated cells (Table 3). Notably, other trends are evident (Tables 4 and 5). The overall rates of apoptosis were quite low (most ranging from 1-5%) making statistical differences in the AI difficult to interpret biologically. No single culture sample showed significant results for both proliferation and apoptosis. In addition, there was no indication that gender played a role in determining response to steroid hormone receptor ligands for either proliferation or apoptosis. Since only a few statistically significant *in vitro* effects were seen with steroid hormones on neurofibroma-derived Schwann cell cultures, perhaps the tumor environment and/or the surrounding cells are necessary to contribute to more dramatic steroid hormone effects on neurofibromas *in vivo*. Also, perhaps both mechanisms leading to increased cell mass (decreased apoptosis and increased proliferation) are utilized in slow-growing neurofibromas, independently or together.

Overall, these data support the hypothesis that steroid hormone receptors are moderately differentially expressed in neurofibromas compared to normal Schwann cell cultures. In addition, there are some effects from treatment with ligands for these receptors on neurofibroma-derived Schwann cell proliferation and survival *in vitro,* but these are small. However, it is conceivable that over time these minor effects might accumulate to contribute to tumor growth. Given the clinical data, we hypothesized that 17β-estradiol and progesterone would cause significant increases in proliferation or decreases in apoptosis. With a few exceptions, most of the statistically significant decreases in proliferation rates were with receptor antagonists. Perhaps these ligands can be used in therapeutic design to slow or prevent tumor growth. The one significant apoptosis result was an increase, and most of the trends are towards the same direction. These observations do not fit a simplistic or global model very well; however, the data support that these receptors are present and active at low levels in normal Schwann cells and neurofibroma-derived Schwann cells and have the potential to contribute to tumor progression. These responses appear to be patient- and possibly tumor-specific. This is also consistent with anecdotal clinical data that not all patients develop neurofibromas during puberty and not all neurofibromas change during hormonal alterations. Heterogeneity among tumors of the same type is being described more often in the literature especially with regards to gene expression profiles. For example, tissue from metastatic prostate carcinomas show different gene expression patterns with array data between patients and even in tissue from different sites in the same patient [30]. In addition, pediatric medulloblastomas show intercellular differences of gene expression and methylation patterns of the MGMT DNA repair gene [31]. Given these data, it is not unexpected to find heterogeneous expression patterns or functional responses within human neurofibroma-derived Schwann cell cultures. This is a very important observation for consideration of NF1 therapies affecting the steroid hormone pathways.

It is also plausible that the Schwann cell does not act alone in response to hormones. The surrounding cells may be important for that effect, and there are likely also other factors unique to each tumor (not unexpected, given that other genetic and epigentic alterations are believed to exist in many of these samples [32, 33]). However, it is feasible that the small changes we observe do contribute to biological effects, which are not quite as dramatic as seen in studies such as in breast cancer. Further work, such as *in vivo* analysis, will help elucidate the effect of steroid hormones on Schwann cells and neurofibromas, leading to a better understanding of the association between these hormones and neurofibroma development and growth. It is conceivable that future therapy may be individualized for a tumor, depending on its steroid hormone characteristics.

Acknowledgements

We acknowledge the UF McKnight Brain Institute for access to the LightCycler, the UF Center for Mammalian Genetics for access to other key equipment and space, equipment purchases through the Children's Miracle Network, and technical assistance by Frederick Kweh. We also thank the physicians and patients who contributed samples used in this research, especially Dr. Hubert Weinberg and Dr. Mark Scarborough. We also thank the National Neurofibromatosis Foundation (Children's Tumor Foundation) for encouraging this research.

References

1. Wallace, MR, Marchuk, DA, Anderson, et al. Type 1 Neurofibromatosis gene: Identification of a large transcript disrupted in three NF1 patients. Science 1990; 249(4965): 181-186.

2. Viskochil, D, Buchberg, AM, Xu, G, et al. Deletions and a translocation interrupt a cloned gene at the Neurofibromatosis type 1 locus. Cell 1990; 62: 187-192.

3. Cawthon, RM, Weiss, R, Xu, G, et al. A major segment of the Neurofibromatosis type 1 gene: cDNA sequence, genomic structures, and point mutations. Cell 1990; 62: 193-201.

4. Dugoff, L and Sujansky, E. Neurofibromatosis type 1 and pregnancy. Am J Med Genet 1996; 66(1): 7-10.

5. Lammert, M, Mautner, V-F and Kluwe, L. Do hormonal contraceptives stimulate growth of neurofibromas? A survey of 59 NF1 patients. BMC Cancer 2005; 5: 16-19.

6. Puls, LE and Chandler, PA. Malignant schwannoma in pregnancy. Acta Obstet Gynecol Scand 1991; 10(3): 243-244.

7. Posma, E, Aalbers, R, Kurniawan, YS, van Essen, AJ, Peeters, PMJG and van Loo, AJ. Neurofibromatosis type 1 and pregnancy: a fatal attraction? Development of malignant schwannoma during pregnancy in a patient with neurofibromatosis type 1. BJOG: Intern J Obstet Gyn 2003; 110: 530-532.

8. Jung-Testas, I, Schumacher, M, Bugnard, H, and Baulieu, EE. Stimulation of rat schwann cell proliferation by estradiol: synergism between the estrogen and cAMP. Dev Brain Res 1993; 72: 282-290.

9. Jung-Testas, I, Schumacher, M, Robel, P and Baulieu, EE. Demonstration of progesterone receptors in rat Schwann cells. J Steroid Biochem Mol Biol 1996; 58(1): 77-82.

10. Koenig, HL, Schumacher, M, Ferzaz, B, et al. Progesterone synthesis and myelin formation by Schwann cells. Science 1995; 268: 1500-1503.

11. Chan, JR, Rodriguez-Waitkus, PM, Ng, BK, Liang, P and Glaser, M. Progesterone synthesized by Schwann cells during myelin formation regulates neuronal gene expression. Mol Biol Cell 2000; 11: 2283-2295.

12. Jung-Testas, I and Baulieu, EE. Steroid hormone receptors and steroid action in rat glial cells of the central and peripheral nervous system. J Steroid Biochem Mol Biol 1998; 65(1-6): 243-251.

13. Svenningsen, AF and Kanje, M. Estrogen and progesterone stimulate Schwann cell proliferation in a sex- and age-dependent manner. J Neurosci Res 1999; 57: 124-130.

14. Martuza, RL, MacLaughlin, DT and Ojemann, RG. Specific estradiol binding in schwannomas, meningiomas and neurofibromas. Neurosurgery 1981; 9(6): 665-670.

15. Chaudhuri, PK, Walker, MJ, Das Gupta, TK and Beattie, CW. Steroid receptors in tumors of nerve sheath origin. J Surg Oncol 1982; 20: 205-206.

16. McLaughlin, ME and Jacks, T. Progesterone receptor expression in neurofibromas. Cancer Res 2003; 63: 752-755.

17. Muir, D, Neubauer, D, Lim, IT, Yachnis, AT and Wallace, MR. Tumorigenic properties of neurofibromin-deficient neurofibroma Schwann cells. Am J Pathol 2001; 158: 501-513.

18. Stumpf, DA, Alksne, JF, Annegers, JF, et al. Neurofibromatosis. Conference Statement. National Institutes of Health Consensus Development Conference. Arch Neurol 1988; 45: 575-578.

19. Campbell-Thompson, M, Lynch, IJ, and Bhardwaj, B. Expression of estrogen receptor (ER) subytpes and ERbeta isoforms in colon cancer. Cancer Res 2001; 61(2): 632-640.

20. Buteau-Lozano, H, Ancelin, M, Lardeux, B, Milanini, J and Perrot-Applanat, M. Transcriptional regulation of vascular endothelial growth factor by estradiol and tamoxifen in breast cancer cells: A complex interplay between estrogen receptors α and β. Cancer Res 2002; 62: 4977-4984.

21. Namiki, M, Yokokawa, K, Okuyama, A, et al. Evidence for the presence of androgen receptors in human Leydig cells. J Steroid Biochem Mol Biol 1991; 38(1): 79-82.

22. Pernas-Alonso, R, Morelli, F, di Porzio, U and Perrone-Capano, C. Multiplex semi-quantitative reverse transcriptase-polymerase chain reaction of low abundance neuronal mRNAs. Brain Res Protocols 1999; 4: 395-406.

23. Mabuchi, S, Ohmichi, M, Kimura, A, et al. Tamoxifen inhibits cell proliferation via mitogen-activated protein kinase cascades in human ovarian cancer cell lines in a manner not dependent on the expression of estrogen receptor or the sensitivity to cisplatin. Endocrinology 2004; 145(3): 1302-1313.

24. Ercoli, A, Scambia, G, Fattorossi, A, et al. Comparative study on the induction of cytostasis and apoptosis by ICI 182,780 and tamoxifen in an estrogen receptor-negative ovarian cancer cell line. Int J Cancer 1998; 76: 47-54.

25. Briand, P, Lundholt, BK, Skouv, J and Lykkesfeldt, AE. Growth response of breast epithelial cells to estrogen is influenced by EGF. Mol Cell Endocrinol 1999; 153(1-2): 1-9.

26. DeClue, JE, Heffelfinger, S, Benvenuto, G, et al. Epidermal growth factor receptor expression in neurofibromatosis type 1- related tumors and NF1 animal models. J Clin Invest 2000; 105: 1233-1241.

27. Rosenbaum, C, Karyala, S, Marchionni, MA, et al. Schwann cells express NDF and SMDF/n-ARIA mRNAs, secrete neuregulin, and show constitutive activation of erbB3 receptors: evidence for a neuregulin autocrine loop. Exp Neurol 1997; 148: 604-615.

28. Sherman, L, Sleeman, JP, Hennigan, RF, Herrlich, P and Ratner, N. Overexpression of activated neu/erbB2 initiates immortalization and malignant transformation of immature Schwann cells in vitro. Oncogene 1999; 18: 6692-6699.

29. Nakamura, T, Ushijima, T, Ishizaka, Y, et al. neu proto-oncogene mutation is specific for the neurofibromas in a N-Nitroso-N-ethylurea-induced hamster neurofibromatosis model but not for hamster melanomas and human Schwann cell tumors. Cancer Res 1994; 54: 976-980.

30. Shah, RB, Mehra, R, Chinnaiyan, AM, et al. Androgen-independent prostate cancer is a heterogeneous group of diseases: lessons from a rapid autopsy program. Cancer Res 2004; 64: 9209-9216.

31. Rood, BR, Zhang, H and Cogen, PH. Intercellular heterogeneity of expression of the MGMT DNA repair gene in pediatric medulloblastoma. Neuro-oncol 2004; 6(3): 200-207.

32. Wallace, MR, Rasmussen, SA, Lim, IT, Gray, BA, Zori, RT and Muir, D. Culture of cytogenetically abnormal Schwann cells from benign and malignant NF1 tumors. Genes Chromosomes Cancer 2000; 27(2): 117-123.

33. Fishbein, L, Eady, B, Sanek, N, Muir, D and Wallace, MR. Analysis of somatic NF1 promoter methylation in plexiform neurofibromas and Schwann cells. Cancer Genet Cytogenet 2005; 157(2): 181-186.

Table 1. Real-time PCR primers.

Gene	PCR Primer Name and Sequence	Annealing Temperature
Estrogen Receptor alpha (*ERα*)	ERα2F 5'-CAT GAT GAA TCT GCA GGG AGA G-3' ERα2R 5'-CCA TCA GGT GGA TCA AAG TGT C-3'	66°C
Estrogen Receptor beta (*ERβ*)	ERβ2F 5'-CTG GTG TGA AGC AAG ATC GC-3' ERβ2R 5'-GCA GAA GTG AGC ATC CCT CTT T-3'	62°C
Progesterone Receptor (*PR*)	PR-F 5'-TCA TTA TGC CTT ACC ATG TGG C-3' PR-R 5'-CTG TGA GCT CGA CAC AAC TCC T-3'	66°C
Androgen Receptor (*AR*)	AR-F 5'-CTA TCC CAG TCC CAC TTG TGT C-3' AR-R 5'-GCT CTT TTG AAG AAG ACC TTG C-3'	66°C
Epidermal Growth Factor Receptor (*EGFR*)	EGFR-F 5'-GGA GAG GAG AAC TGC CAG AAA C-3' EGFR-R 5'- GTG GCA CCA AAG CTG TAT TTG C-3'	59°C
ERBB2 (*HER2/neu*)	ERBB2-2F 5'-CAG CCT TGC CCC ATC AAC TGC-3' NEUB 5'-CGT TTC CTG CAG CAG TCT CC-3'	69°C
Vascular Endothelial Growth Factor (*VEGF*)	VEGFex1F 5'-CGA AAC CAT GAA CTT TCT GC-3' VEGFex3R 5'-CCT CAG TGG GCA CAC ACT CC-3'	55°C
Hypoxanthine Phosphoribosyl Transferase (*HPRT*)	HPRTupper 5'-CCT GCT GGA TTA CAT TAA AGC ACT G-3' HPRTlower 5'-CCT GAA GTA CTC ATT ATA GTC AAG G-3'	60°C

Table 2. Real-time PCR ratios of steroid hormone receptor expression in neurofibromas compared to normal Schwann cells.

Tumor Type	Samples	ER alpha	ER beta	PR	AR
Dermal cultures					
F*	UF 328T8c (cNF96.5g)	--	UD†	+10%	+10%
F	UF 470T1c (cNF97.2a)	UD	UD	UD	+20%
M	UF 505T3c (cNF98.4a)	-10%	--	+10%	+10%
M	UF 505T7c (cNF98.4d)	--	-10%	+10%	+10%
M	UF 475Tc (cNF97.5)	-10%	--	UD	--
F	UF 532T1c (cNF99.1)	+10%	UD	+20%	+20%
M	UF 17T1c (cNF00.10a)	--	UD	UD	-10%
M	UF 17T2c (cNF00.10b)	--	UD	UD	-20%
Plexiform cultures					
M	UF 378T2bc (pNF95.11b)	-20%	--	--	+10%
M	UF 362T1c (pNF95.6)	UD	UD	-20%	+10%
F	UF 440Tc (pNF97.9)	--	UD	+20%	+10%
F	UF 511T2c (pNF98.3)	--	UD	-10%	-10%
F	UF 554T1c (pNF99.5)	UD	UD	UD	-20%
F	UF 572Tc (pNF00.6)	--	UD	--	-10%
F	UF 593T1c (pNF00.8)	--	UD	+10%	--
F	UF 836Tc (pNF02.6)	--	UD	--	+10%
F	UF 550Tc (pNF99.4)	+10%	UD	+10%	+40%
F	UF 746Tc (pNF01.1)	UD	UD	--	+10%
MPNST cultures					
M	UF 459Tc (sNF96.2)	UD	UD	UD	+20%
F	UF 302Tc (sNF94.3)	-30%	-10%	+20%	+30%
Controls					
	MCF7	+50%	NT‡	+60%	UD
	Testis	NT	UD	NT	+20%
	Caco2	UD	+20%	UD	NT

*M/F =derived from a male or female patient, respectively

†UD =no expression detected

‡NT =not tested; (--)= no change from normal Schwann cells

ER, PR, AR=estrogen, progesterone, and androgen receptors, respectively; MPNST=malignant peripheral nerve sheath tumor

Table 2. Continued.

Tumor Type	Samples	ER alpha	ER beta	PR	AR
Primary dermal tumors					
F*	UF 328T7	+10%	UD†	+90%	+40%
M	UF 17T1	+10%	+10%	+20%	-10%
M	UF 17T2	+10%	+10%	+30%	+10%
F	UF 80T2	+30%	UD	+70%	+40%
F	UF 80T6	+30%	UD	+60%	+50%
M	UF 158T3	+20%	+20%	+40%	+20%
M	UF 486T1	+10%	--	+50%	--
M	UF 486T5	+30%	+10%	+70%	+10%
F	UF 495T2	+30%	+20%	+50%	+20%
F	UF 495T3	+30%	+20%	+40%	+20%
M	UF 505T3	UD	+10%	+50%	+30%
M	UF 505T7	+30%	+10%	+60%	+40%
F	UF 532T1	UD	UD	UD	+60%
F	UF 549T	UD	UD	+60%	+40%
M	UF 743T1	+20%	+20%	+40%	+20%
M	UF 743T2	+30%	+20%	+50%	+20%
M	UF 743T4	+20%	+20%	+40%	+10%
Primary plexiform tumors					
M	UF 362T	UD	+20%	+50%	+60%
F	UF 154T	+30%	+10%	+60%	+30%
F	UF 429T	+20%	+20%	+40%	+20%
F	UF 537T	UD	UD	+30%	--
F	UF 714T	+20%	+20%	+30%	+20%
F	UF 746T1	+40%	+10%	+70%	+50%
M	UF 787T1	+20%	UD	+60%	+40%
M	UF 378T2b	UD	--	+40%	+40%
F	UF 572T1	+10%	+20%	UD	--
F	UF 550T1	UD	+10%	+40%	+10%
Primary MPNSTs					
M	UF 459T	+10%	+10%	+10%	--
M	UF 820T	--	+10%	+30%	+10%

*M/F =derived from a male or female patient, respectively

†(UD) =no expression detected

‡NT =not tested; (--) =no change from normal Schwann cells

Table 3. Statistically significant alterations in proliferation and apoptosis in normal Schwann cells and neurofibroma-derived Schwann cell cultures in response to steroid hormone ligands.

Gender	Sample	17β-estradiol	ICI 182,780	Mifepristone	Tamoxifen
F	pn02.3	--	↓P*(52.2%)	--	↓P(61.0%)
M	cNF97.5	--	--	↑P(136.3%)	--
F	cNF99.1	--	↓P(28.5%)	--	--
M	pNF00.11	--	--	--	↓P(53.0%)
F	pNF00.13	--	--	--	↑P(155.5%)
F	pNF99.5	↑A(280.0%)	--	--	--

*↑/↓P, A(average % of no-treatment control)=increase or decrease in PI or AI (as a percent of no-treatment control) with $p<0.05$; (--)=no change

pn=normal Schwann cell cultures; cNF=dermal cultures; pNF=plexiform cultures;

M, F=derived from male or female patient, respectively

Table 4. Trends in proliferation in normal Schwann cells and neurofibroma-derived Schwann cell cultures in response to steroid hormone ligands.

Gender	Sample	17β-estradiol	Progesterone	ICI 182,780	Mifepristone	Tamoxifen
M	pn02.8	--	↓*	--	--	--
M	pn97.4	↑	--	--	↑	↓
F	pn02.3	--	--	--	--	--
F	pn02.7	↓	--	--	↓	↑
M	cNF97.5	--	--	--	↑	--
M	cNF98.4d	--	--	↑	↑	--
F	cNF99.1	--	--	↓	↑	--
F	cNF96.5f	↓	↑	--	↓	--
F	cNF97.2a	--	↓	--	--	--
F	cNF97.2b	--	--	--	--	--
M	pNF00.11	--	↓	--	--	↓
M	pNF95.11b	↑	↓	--	--	
M	pNF95.6	--	--	↓	↓	↓
F	pNF00.13	↑	--	--	--	--
F	pNF01.1	--	--	↓	--	↓
F	pNF99.5	--	--	--	--	--
F	pNF02.6	↑	↑	↑	--	↑
M	sNF02.2	--	--	↓	--	--
M	sNF96.2	--	--	--	--	--

*↑/↓=increase or decrease ≥10% relative to no-treatment control; (--)=no change

pn=normal Schwann cell cultures; cNF=dermal cultures; pNF=plexiform cultures; sNF=MPNST cultures; M, F=derived from male or female patient, respectively

Table 5. Trends in apoptosis in normal Schwann cells and neurofibroma-derived Schwann cell cultures in response to steroid hormone ligands.

Gender	Sample	17β-estradiol	Progesterone	ICI 182,780	Mifepristone	Tamoxifen
M	pn02.8	--	--	↑*	--	↓
M	pn97.4	--	--	--	↑	↑
F	pn02.3	--	--	--	↓	↓
F	pn02.7	--	--	--	--	--
M	cNF97.5	↓	--	↑	--	--
M	cNF98.4d	--	↓	--	↓	--
F	cNF99.1	--	--	--	↑	↑
F	cNF96.5f	--	↓	--	↓	--
F	cNF97.2a	--	--	--	--	--
F	cNF97.2b	--	↓	--	↓	--
M	pNF00.11	--	--	--	↓	--
M	pNF95.11b	--	--	--	--	↑
M	pNF95.6	--	--	↑	↑	↑
F	pNF00.13	↑	↑	--	↑	--
F	pNF01.1	--	--	--	--	--
F	pNF99.5	↑	↑	↑	--	↑
F	pNF02.6	↑	--	--	--	--
M	sNF02.2	↑	--	↑	↑	--
M	sNF96.2	--	↑	--	↑	↑

*↑/↓-=increase or decrease ≥10% relative to no-treatment control; (--)=no change

pn=normal Schwann cell cultures; cNF=dermal cultures; pNF=plexiform cultures; sNF=MPNST cultures; M, F=derived from male or female patient, respectively

Legends for Illustrations

Figure 1. PR immunohistochemistry (200x magnification). Panel A represents one of 38 neurofibromas which showed PR positive staining. Panel B represents a negative control of neurofibroma tissue. Panel C represents a known PR positive control (breast carcinoma tissue).

Figure 2. TUNEL and BrdU staining. Photos show samples (200x magnification) from the normal Schwann cell culture pn97.4 for the (A) TUNEL assay to detect apoptosis (AI=5.6%) and the (B) BrdU proliferation assay (PI=30.4%). Asterisks (*) denote positively stained cells.

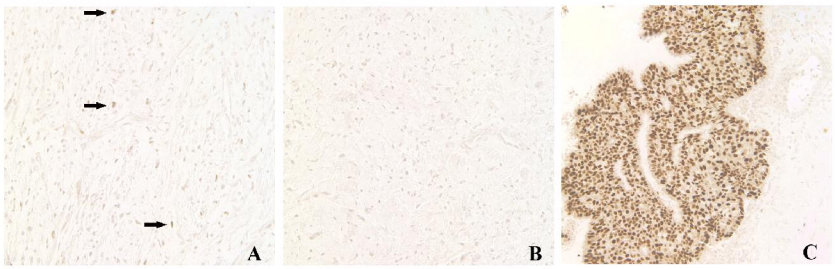

Figure 1. PR immunohistochemistry (200x magnification). Panel A represents one of 38 neurofibromas which showed PR positive staining. Panel B represents a negative control of neurofibroma tissue. Panel C represents a known PR positive control (breast carcinoma tissue).

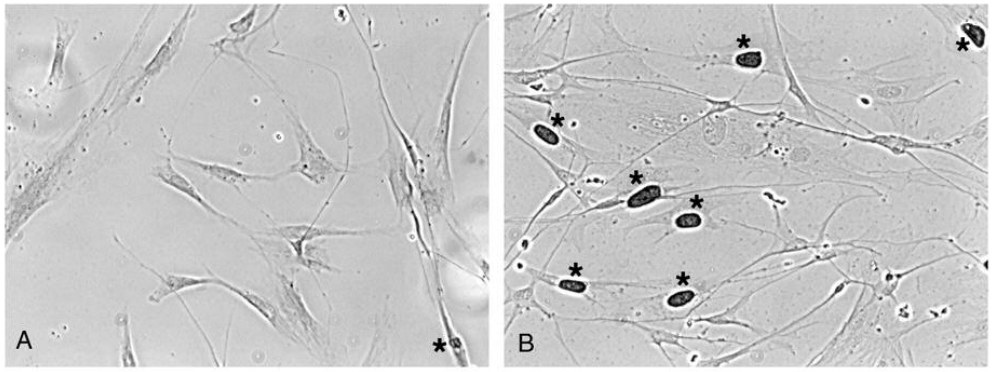

Figure 2. TUNEL and BrdU staining. Photos show samples (200x magnification) from the normal Schwann cell culture pn97.4 for the (A) TUNEL assay to detect apoptosis (AI=5.6%) and the (B) BrdU proliferation assay (PI=30.4%). Asterisks (*) denote positively stained cells.